Genetic identification of thiosulfate sulfurtransferase as an adipocyte-expressed antidiabetic target in...

Article *in* Nature Medicine · June 2016

DOI: 10.1038/nm.4115

nature medicine

Genetic identification of thiosulfate sulfurtransferase as an adipocyte-expressed antidiabetic target in mice selected for leanness

Nicholas M Morton[1], Jasmina Beltram[2], Roderick N Carter[1], Zoi Michailidou[1], Gregor Gorjanc[2], Clare McFadden[1], Martin E Barrios-Llerena[1], Sergio Rodriguez-Cuenca[3], Matthew T G Gibbins[1], Rhona E Aird[1], José Maria Moreno-Navarrete[4–6], Steven C Munger[7], Karen L Svenson[7], Annalisa Gastaldello[1], Lynne Ramage[1], Gregorio Naredo[1], Maximilian Zeyda[8], Zhao V Wang[9], Alexander F Howie[10], Aila Saari[11], Petra Sipilä[12], Thomas M Stulnig[8], Vilmundur Gudnason[13], Christopher J Kenyon[1], Jonathan R Seckl[1], Brian R Walker[1], Scott P Webster[1], Donald R Dunbar[1], Gary A Churchill[7], Antonio Vidal-Puig[3,14], José Manuel Fernandez-Real[4–6], Valur Emilsson[13,15] & Simon Horvat[2,16]

The discovery of genetic mechanisms for resistance to obesity and diabetes may illuminate new therapeutic strategies for the treatment of this global health challenge. We used the polygenic 'lean' mouse model, which has been selected for low adiposity over 60 generations, to identify mitochondrial thiosulfate sulfurtransferase (*Tst*; also known as rhodanese) as a candidate obesity-resistance gene with selectively increased expression in adipocytes. Elevated adipose *Tst* expression correlated with indices of metabolic health across diverse mouse strains. Transgenic overexpression of *Tst* in adipocytes protected mice from diet-induced obesity and insulin-resistant diabetes. *Tst*-deficient mice showed markedly exacerbated diabetes, whereas pharmacological activation of TST ameliorated diabetes in mice. Mechanistically, TST selectively augmented mitochondrial function combined with degradation of reactive oxygen species and sulfide. In humans, *TST* mRNA expression in adipose tissue correlated positively with insulin sensitivity in adipose tissue and negatively with fat mass. Thus, the genetic identification of *Tst* as a beneficial regulator of adipocyte mitochondrial function may have therapeutic significance for individuals with type 2 diabetes.

Obesity prevalence seems to have plateaued at ~40% (refs. 1,2), suggesting that environmental penetrance (such as a hypercaloric diet or a sedentary lifestyle) is limited to a subpopulation of individuals who are genetically susceptible to obesity. Indeed, a substantial and stable proportion of the population has remained non-obese despite the modern obesogenic onslaught[3]. Determining the genetic basis for this resilience may illuminate novel intervention strategies for obesity and its associated cardiometabolic diseases. To discover novel genes that contribute to healthy low adiposity, we used a unique polygenic lean mouse line that was generated through selection for low adiposity over 60 generations. Lean mice (in which 4% of body weight is fat mass) show metabolically healthy leanness[4], not lipodystrophy. The major quantitative trait loci (QTL) underlying divergent adiposity between lean mice and their counter-selected 'fat' mouse line (in which 23% of body weight is fat mass) have been described[5,6], which facilitated our search for positional candidate lean genes. Direct experimental evidence[7] and QTL mapping also ruled out genes in known brain-regulated appetite and energy expenditure systems—such as leptin (*Lep*), leptin receptor (*Lepr*), neuropeptide Y (*Npy*) and melanocortin 4 receptor (*Mc4r*)—as drivers of adiposity divergence. Lean mice thus allow for insight into the genetic landscape of healthy leanness that is likely manifested through peripheral mechanisms. We reasoned that selection on adiposity divergence, independently of lean mass, would enrich for genes with direct actions in the adipose tissue. To identify adipose-tissue-specific candidate lean genes, strict inclusion criteria were applied to transcriptomic profiles from three distinct white

[1]University–British Heart Foundation Centre for Cardiovascular Science, University of Edinburgh, Queen's Medical Research Institute, Edinburgh, UK. [2]Biotechnical Faculty, Animal Science Department, University of Ljubljana, Ljubljana, Slovenia. [3]Metabolic Research Laboratories, Level 4, Wellcome Trust–MRC Institute of Metabolic Science, Addenbrookes Hospital, Cambridge, UK. [4]Department of Diabetes, Endocrinology and Nutrition, Institut d'Investigació Biomédica de Girona, Girona, Spain. [5]Department of Medicine, University of Girona, Girona, Spain. [6]Centro de Investigación Biomédica en Red de Fisiopatología de la Obesidad y Nutrición, Instituto de Salud Carlos III, Girona, Spain. [7]The Jackson Laboratory, Bar Harbor, Maine, USA. [8]Clinical Division of Endocrinology and Metabolism, Department of Medicine III, Medical University of Vienna, Vienna, Austria. [9]Department of Internal Medicine, Touchstone Diabetes Center, University of Texas Southwestern Medical Center, Dallas, Texas, USA. [10]The Medical Research Council (MRC) Centre for Reproductive Health, University of Edinburgh, Queen's Medical Research Institute, Edinburgh, UK. [11]Department of Physiology, Institute of Biomedicine, University of Turku, Turku, Finland. [12]Central Animal Laboratory, University of Turku, Turku, Finland. [13]Icelandic Heart Association, Kopavogur, Iceland. [14]Wellcome Trust Sanger Institute, Wellcome Trust Genome Campus, Hinxton, Cambridge, UK. [15]Faculty of Pharmaceutical Sciences, University of Iceland, Reykjavik, Iceland. [16]National Institute of Chemistry, Ljubljana, Slovenia. Correspondence should be addressed to N.M.M. (nik.morton@ed.ac.uk) or S.H. (simon.horvat@bf.uni-lj.si).

Received 19 December 2015; accepted 29 April 2016; published online 6 June 2016; doi:10.1038/nm.4115

adipose tissue (WAT) depots (subcutaneous, epididymal and mesenteric) versus those from liver, muscle and kidney of the lean and fat mice. mRNAs that showed coordinate elevation in only the WAT depots from lean mice were then prioritized by using adiposity QTL information. Genetic and functional validation supported nuclear-encoded mitochondrial *Tst* as a novel lean line adiposity-reducing gene with a dominant and broader influence on resistance to metabolic disease across species.

RESULTS

Elevated adipose *Tst* expression links leanness and metabolic health

To prioritize positional candidate lean genes from within major adiposity QTLs[5,6], we selected mRNAs whose levels were increased specifically in the WAT of lean mice[8]. To be considered a candidate gene, mRNA levels had to be >2-fold higher in all three WAT depots—but comparable in the liver, muscle and kidney—of lean versus fat mice. In an independent microarray experiment, we validated that there were higher levels of *Tst* mRNA in the subcutaneous WAT of lean versus fat mice. Eleven genes fulfilled the tissue-specific expression criteria (expressed sequence tag (EST) AI427515, *Csprs*, *Cyp2e1*, *Fv1*, *Ms4a4c*, *Ms4a6c*, *Pik3cg*, *Pon1*, *Rassf6*, *Sah* and *Tst*), and two genes fulfilled the QTL inclusion criteria (*Pik3cg* on chromosome 12 and *Tst* on chromosome 15). *Pik3cg* failed validation in the independent microarray experiment. Only the nuclear-encoded *Tst* gene, which is positioned on chromosome 15 (78,399,556–78,405,859) within the F-line obesity QTL 3 (*Fob3*)[5,6], fulfilled all of our inclusion criteria. *Tst* mRNA was ~7-fold higher across the three WAT depots in lean versus fat mice (**Fig. 1a**).

To support causality—and not just a simple association—with leanness, we sought evidence that increased *Tst* mRNA originated from a *cis*-acting effect within the QTL. To this end we used congenic lines of mice that had increasingly refined lean-line *Fob3* QTL chromosome 15 segments around the *Tst* locus introgressed into an otherwise fat-line genetic background (lines U12, M and M2). The U12 line carries a ~35-Mbp QTL (*Fob3b*) that accounted for a 20% reduction in adiposity of the fat mouse line[5]. The M line carries a ~6.8-Mbp sub-QTL (*Fob3b2*)[6] that accounted for an 8.1% reduction in the adiposity of the fat mice (**Supplementary Table 1a**). The M2 line was developed specifically for this study and carries a ~2.8-Mbp

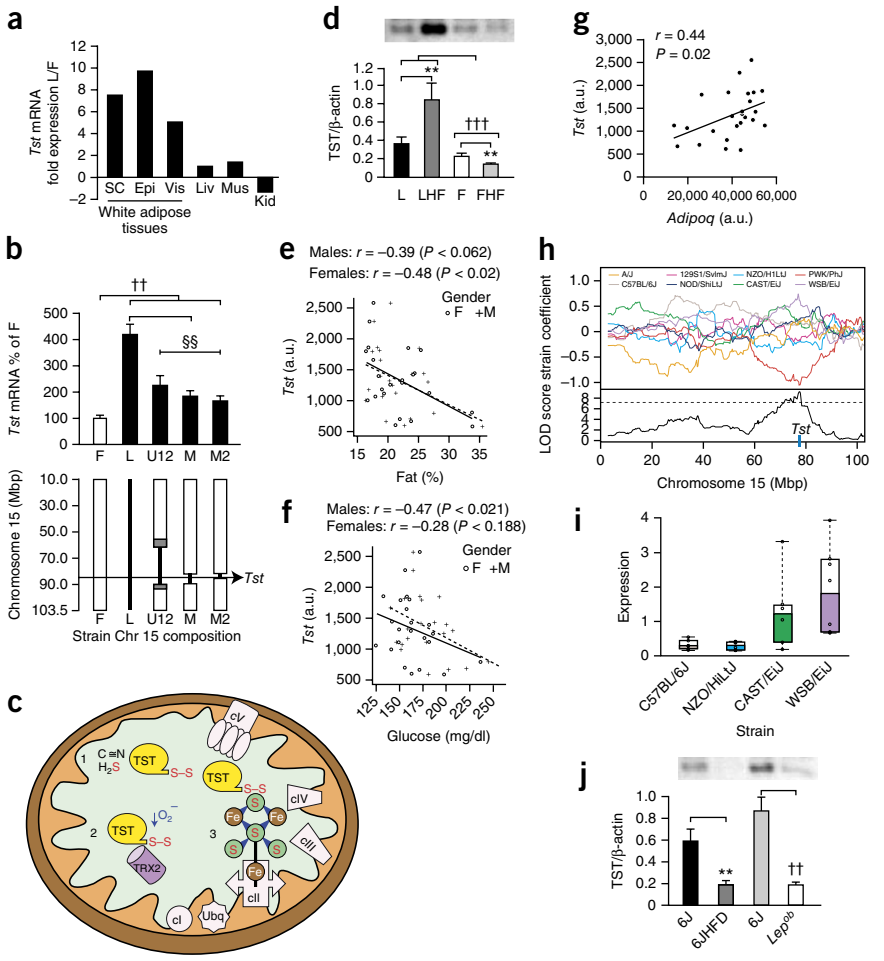

Figure 1 TST is elevated in adipose tissues from lean mice. (**a**) Ratio of *Tst* mRNA levels ($n = 3$ mice per group) in lean (L) versus fat (F) mice in tissue from subcutaneous (SC), epididymal (Epi) and visceral (Vis) fat or from liver (Liv), muscle (Mus) and kidney (Kid). (**b**) Top, *Tst* mRNA levels in SC fat from F mice ($n = 16$), L mice ($n = 16$ mice) or the derived congenic lines U12 ($n = 8$ mice), M ($n = 8$ mice) and M2 ($n = 8$ mice). Bottom, chromosome 15 composition derived from F (white), L (black) and origin-undetermined regions (gray). Horizontal arrow indicates position of the *Tst* gene. (**c**) Schematic showing that TST (yellow) modulates cyanide and H_2S (1), ROS (O_2^-) with thioredoxin (TRX2; purple) (2) and respiratory complex (designated 'c') enzymes (such as the cII enzyme, succinate dehydrogenase) (3). Fe-S, iron–sulfur cluster; S, sulfur; S–S, sulfane–sulfur; Ubq, ubiqinone. (**d**) Representative western blot image (of $n = 6$ mice per group) of TST protein (top) and quantification of TST (relative to β-actin) levels (bottom) in SC fat of L mice on a control diet (black) or a HFD (dark gray) and of F mice on a control diet (white bars) or a HFD (light gray bars). (**e**–**g**) Adipose *Tst* mRNA correlations (Pearson's) with fat mass (**e**), blood glucose (**f**) or adiponectin mRNA (**g**) levels across 23 mouse strains. (**h**) *Tst* expression from segregating *Tst* locus in the Diversity Outbred (DO) strains ($n = 277$ mice) (top) and logarithm of the odds (LOD) score (bottom) for a combined plot for the data from all strains. Blue bar indicates position of *Tst* on chromosome 15. (**i**) Correlation of *Tst* mRNA levels (as determined by RNA-seq of SC fat tissue) with female adiposity in founder DO strains ($n = 6$ mice per strain; mice were either on a control diet or a HFD. Box plots with dashed bars correspond to minimum and maximum values. Upper and lower borders of the box correspond to the 25th and 75th percentile, respectively). (**j**) Representative western blot (top) and quantification (bottom) of TST expression in the SC fat of C57BL/6J mice that were fed a control diet (6J; black bar; $n = 6$) or a HFD (6JHFD; $n = 6$) for 16 weeks or of 10-week-old C57BL/6J (6J; light gray bar, $n = 6$) and leptin-deficient (*Lep*^{ob}) ($n = 5$) mice that were both fed a control diet. In **a**,**b**,**d**,**j**, data are mean ± s.e.m. In **b**, $^{\dagger\dagger}P < 0.01$ versus F mice, and $^{\S\S}P < 0.01$ versus L mice, by one-way analysis of variance (ANOVA). In **d**,**j**, $^{**}P < 0.01$ (effect of diet), and $^{\dagger\dagger}P < 0.01$ and $^{\dagger\dagger\dagger}P < 0.001$ (effect of line or genotype), by two-way ANOVA.

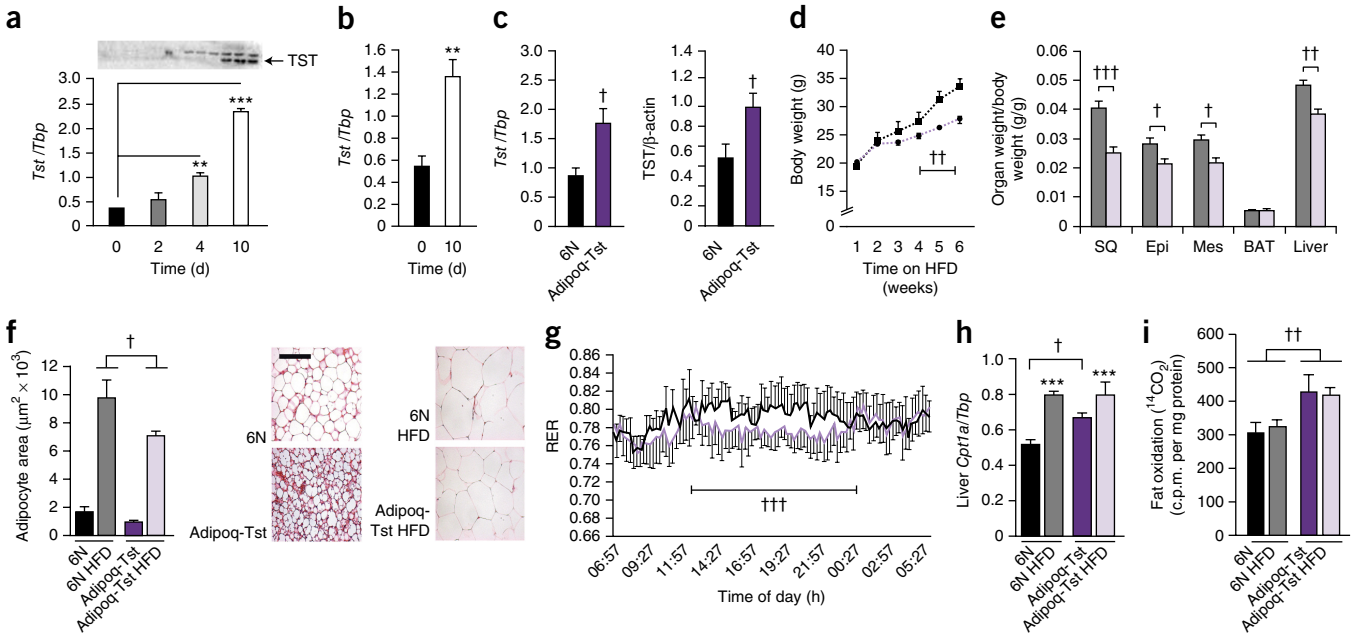

Figure 2 *Tst* overexpression in adipocytes drives obesity resistance. (**a**) Western blot analysis ($n = 3$ samples per time point) of TST protein (top) and quantification of *Tst* mRNA levels ($n = 3$ samples per time point) (bottom) in differentiating 3T3-L1 preadipocytes. $^{**}P < 0.01$ and $^{***}P < 0.001$ by one-way ANOVA. (**b**) *Tst* mRNA levels in cultured mouse SVFs at day 0 and after 10 d of differentiation ($n = 3$ samples per time point). $^{**}P < 0.01$ by Student's *t*-test. (**c**) Quantification of *Tst* mRNA (left) and TST protein (right) levels in the WAT of C57BL/6N control (6N) or Adipoq-Tst mice ($n = 5$ mice per group). $^{\dagger}P < 0.05$ by Student's *t*-test. (**d**) Weights of C57BL/6N (squares) or Adipoq-Tst (circles) mice that were fed a HFD for 6 weeks ($n = 5$ mice per group). $^{\dagger\dagger}P < 0.01$ by repeated-measures (RM) ANOVA. (**e**) Weight of the indicated organs (relative to body weight (BW)) of C57BL/6N (gray bars; $n = 4$ mice) or Adipoq-Tst (purple bars; $n = 5$ mice) mice after 6 weeks on a HFD. $^{\dagger}P < 0.05$, $^{\dagger\dagger}P < 0.01$ and $^{\dagger\dagger\dagger}P < 0.001$ by two-way ANOVA. (**f**) Quantification of fat cell size (graph; left) and representative images of adipose sections (right) from C57BL/6N and Adipoq-Tst mice fed either a control diet (6N, $n = 5$; Adipoq-Tst, $n = 6$) or a HFD (6N HFD, $n = 6$; Adipoq-Tst HFD, $n = 6$) for 6 weeks. $^{\dagger}P < 0.01$ effect of genotype by two-way ANOVA. Scale bar, 100 μm. (**g**) Respiratory exchange ratio (RER) in C57BL/6N (black lines) versus Adipoq-Tst (purple lines) mice after 6 weeks on a HFD ($n = 4$ mice per group). $^{\dagger\dagger\dagger}P < 0.001$, effect of genotype (mean RER between 13:00 h and 01:00 h) by Student's *t*-test. (**h**,**i**) Hepatic *Cpt1a* mRNA levels (**h**) and [1-^{14}C]palmitate oxidation. c.p.m., counts per minute (**i**) in groups as described in **f** ($n = 6$ mice per group). $^{***}P < 0.001$ (effect of diet), and $^{\dagger}P < 0.05$ and $^{\dagger\dagger}P < 0.01$ (effect of genotype), by two-way ANOVA. Throughout, data are mean ± s.e.m.

sub-sub-QTL (*Fob3b2-M2*; **Supplementary Fig. 1**) that accounted for an 8.4% reduction in the adiposity of fat mice (**Supplementary Table 1a**). Comparable amounts of fat reduction in the M2 versus the M line suggested that the leanness effect was fully captured by the smallest (sub-sub-QTL) genetic interval (**Supplementary Fig. 1b–e** and **Supplementary Table 1b**). *Tst* mRNA levels in adipose tissue were higher in all three congenic lines than in the parental fat line, supporting *Tst* as a positional candidate lean gene (**Fig. 1b**). Furthermore, in *Fob3b2-M2* heterozygotes, expression of the *Tst* allele originating from lean mice was higher than expression of the allele originating from fat mice (**Supplementary Fig. 1f**,**g**). Given that the *Fob3b2-M2* congenic line carries a ~2.8-Mbp lean-line segment around *Tst*, these allele-dosage studies implicate a *cis*-mediated mechanism underlying increased levels of *Tst* mRNA in lean mice (**Supplementary Fig. 1f**,**g**). Co-segregation of metabolic protection with the lean-line *Tst* allele was confirmed in *Fob3b2-M2* mice (**Supplementary Fig. 1h**,**i**). We used haplotype analysis of the M2 interval to restrict for causal genomic regions (which were non-identical by descent). 20 of 90 genes remained positional candidates, of which only *Tst* showed coordinate upregulation in all three WAT depots from the lean mice (**Fig. 1a**) and in WAT from the *Fob3b2-M2* lean-allele homozygotes that were generated from an F_2 cross with mice from the fat line (**Supplementary Fig. 2**). *Tst* also scored as the top functional and positional candidate gene by bioinformatics approaches (**Supplementary Fig. 2**).

Given the strong genetic evidence for *Tst* as a causal lean gene, we considered the mechanistic rationale for its effects. TST was identified more than 80 years ago as a rhodanese enzyme activity involved in cyanide detoxification[9], with the clinical antidote thiosulfate (S_2O_3) serving as a TST substrate for sulfane–sulfur transfer[9,10]. This did not immediately suggest a purpose for TST in fat cell function or adiposity. TST was, however, linked to the modulation of iron–sulfur (Fe-S) clusters and regulatory cysteine residues in succinate dehydrogenase[11] and to the modulation of NADH dehydrogenase[12], two key mitochondrial respiratory complexes. In addition, TST degraded reactive oxygen species (ROS) with thioredoxin in cell-free systems[13] and participated in sulfide (H_2S) metabolism[14] through its interaction with the sulfur dioxygenase ETHE1 (ref. 15). Unfolded TST may also chaperone cytosolic 5S rRNA to the mitochondria[16]. Because mitochondrial ROS[17–19], and more recently H_2S[20,21], have been implicated in adipocyte function, we hypothesized that elevated TST activity beneficially alters these pathways (**Fig. 1c**).

During the process of validating the candidate lean genes, we found that adipose TST was unexpectedly upregulated in lean mice that were challenged with a high-fat diet (HFD) (**Fig. 1d**). Moreover, the lean mice on the HFD notably lost fat mass (**Supplementary Table 2a**,**b**). We had reported earlier[4] that lean mice on a HFD showed fat loss in a manner that could not be fully explained on the basis of divergent eating or running behavior[7,22], which supported the idea of alternative mechanisms of leanness. By contrast, adipose TST levels were reduced

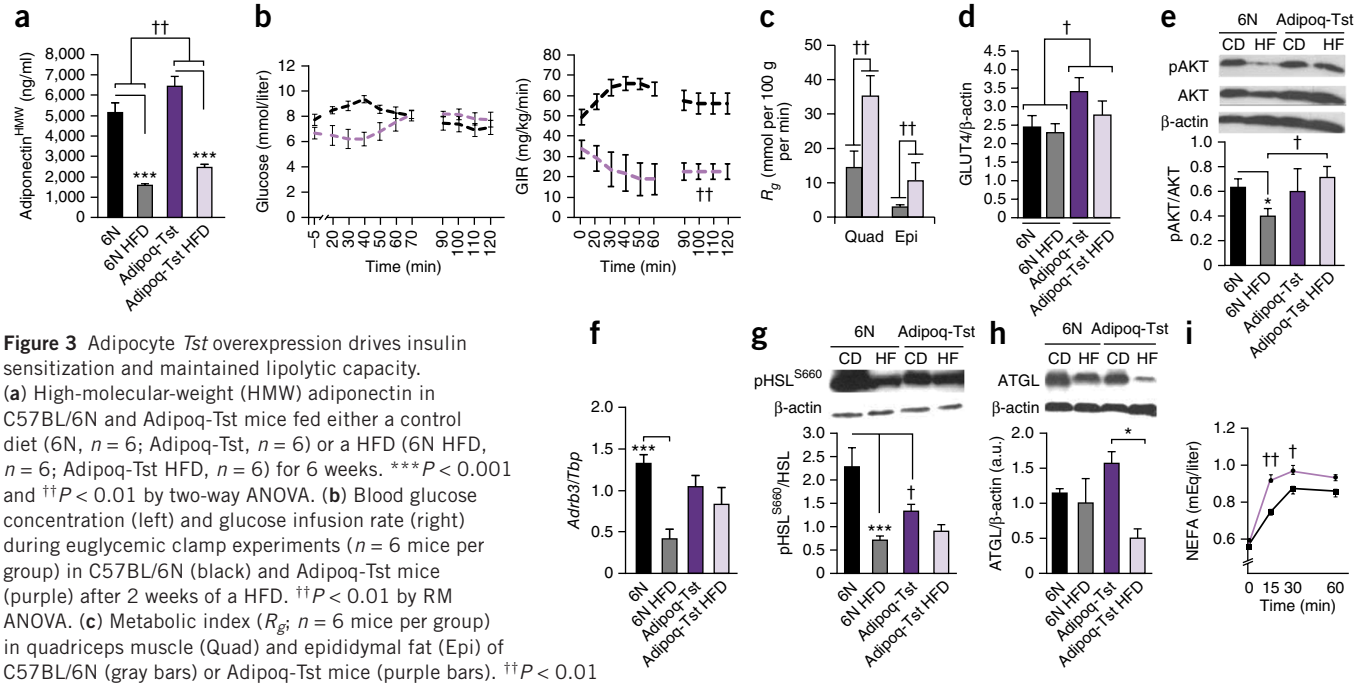

Figure 3 Adipocyte *Tst* overexpression drives insulin sensitization and maintained lipolytic capacity. (**a**) High-molecular-weight (HMW) adiponectin in C57BL/6N and Adipoq-Tst mice fed either a control diet (6N, $n = 6$; Adipoq-Tst, $n = 6$) or a HFD (6N HFD, $n = 6$; Adipoq-Tst HFD, $n = 6$) for 6 weeks. $^{***}P < 0.001$ and $^{††}P < 0.01$ by two-way ANOVA. (**b**) Blood glucose concentration (left) and glucose infusion rate (right) during euglycemic clamp experiments ($n = 6$ mice per group) in C57BL/6N (black) and Adipoq-Tst mice (purple) after 2 weeks of a HFD. $^{††}P < 0.01$ by RM ANOVA. (**c**) Metabolic index (R_g; $n = 6$ mice per group) in quadriceps muscle (Quad) and epididymal fat (Epi) of C57BL/6N (gray bars) or Adipoq-Tst mice (purple bars). $^{††}P < 0.01$ by two-way ANOVA. (**d**) GLUT4 protein levels in mice treated as in **a** (6N, $n = 5$; Adipoq-Tst, $n = 6$; 6N HFD, $n = 5$; Adipoq-Tst HFD, $n = 5$). (**e**) Representative western blot analysis for (top) and quantification of (bottom) the expression of phospho-AKT in mice treated as in **a** (6N, $n = 3$; Adipoq-Tst, $n = 3$; 6N HFD, $n = 4$; Adipoq-Tst HFD, $n = 3$). (**f**) β3-adrenergic receptor (*Adrb3*) mRNA levels in mice treated as in **a** (6N, $n = 5$; Adipoq-Tst, $n = 5$; 6N HFD, $n = 5$; Adipoq-Tst HFD, $n = 6$). (**g**,**h**) Representative western blot analysis for (top) and quantification of (bottom) the expression of pHSL^{S660} (6N, $n = 3$; Adipoq-Tst, $n = 3$; 6N HFD, $n = 4$; Adipoq-Tst HFD, $n = 4$) (**g**) or ATGL protein ($n = 3$ per group) (**h**) for mice treated as in **a**. (**i**) Plasma NEFA levels after CL316,243 administration (1 μg/g) to C57BL/6N (squares, $n = 5$) or Adipoq-Tst (circles, $n = 8$) mice. Throughout, data are mean ± s.e.m. In **c**–**i**, $^{*}P < 0.05$, $^{***}P < 0.001$, $^{†}P < 0.05$ and $^{††}P < 0.01$ by two-way ANOVA (**c**–**h**) or RM ANOVA (**i**).

in fat mice (**Fig. 1d**) that gained fat mass after being fed a HFD (**Supplementary Table 2**). We then investigated whether TST was broadly related to adiposity in mice. *Tst* mRNA levels in adipose tissue correlated negatively with fat mass and plasma glucose levels (**Fig. 1e**,**f**) but positively with adiponectin (*Adipoq*) mRNA across 23 commonly used mouse strains (**Fig. 1g**). RNA sequencing (RNA-seq) data from the Diversity Outbred (DO) panel of mice[23] revealed an expression QTL (eQTL) at the *Tst* locus, whereby *Tst* intervals derived from lean founder mouse strains had higher liver *Tst* mRNA levels (**Fig. 1h**). Higher levels of adipose *Tst* mRNA were also found in representative lean DO founder strains, as compared to those in obesity-susceptible strains (**Fig. 1i** and **Supplementary Fig. 3a**). Levels of adipose *Tst* mRNA (**Supplementary Fig. 3b**,**c**) and TST protein (**Fig. 1j**) were markedly lower in HFD-fed obesity-prone male C57BL/6J mice and in leptin-deficient, C57BL/6J*Lep*$^{ob/ob}$ mice than in their age-matched C57BL/6J controls.

Overexpression of *Tst* in adipocytes preserves metabolic health

We next tested the hypothesis that elevated adipose *Tst* was causal for leanness. We first established that *Tst* was expressed predominantly in mature 3T3-L1 (**Fig. 2a**) and primary adipocytes (**Fig. 2b**). We then generated mice overexpressing *Tst* ~2-fold in the mature adipocytes (**Fig. 2c**) by using the adiponectin promoter[24] (which we refer to as Adipoq-Tst mice). *Tst* mRNA was unchanged in brown adipose tissue (BAT) or bone of Adipoq-Tst mice (**Supplementary Fig. 4a**,**b**). Adipoq-Tst mice were of initially comparable weight to their nontransgenic littermates (**Fig. 2d**), but they resisted HFD-induced obesity (**Fig. 2d**,**e** and **Supplementary Fig. 4c**,**d**) and had smaller fat cells (**Fig. 2f**), despite similar food intake (**Supplementary Fig. 4e**). As compared to C57BL/6N control mice, Adipoq-Tst mice showed higher energy expenditure when fed chow or a HFD (**Supplementary Fig. 4f**,**g**), with a lower respiratory exchange ratio after being fed a HFD—which is indicative of preferential fat oxidation (**Fig. 2g** and **Supplementary Fig. 4g**)—particularly mid-way through the diurnal cycle (**Fig. 2g**). Physical activity was comparable between mice of the two genotypes (**Supplementary Fig. 4h**). Overexpression of *Tst* did not increase the mRNA levels of uncoupling protein 1 (mitochondrial, proton carrier) (*Ucp1*) in the BAT or WAT (**Supplementary Fig. 4i**,**j**), suggesting that WAT beigeing is not a major driver of obesity resistance in Adipoq-Tst mice. Instead, *Tst* overexpression in adipocytes was associated with elevated basal mRNA levels of liver carnitine palmitoyltransferase 1a (*Cpt1a*) (**Fig. 2h**), a key enzyme of fatty acid oxidation, and this was corroborated by increased hepatic fat oxidation in Adipoq-Tst mice as compared to that in littermate control mice (**Fig. 2i**).

We next investigated whether adipocyte *Tst* overexpression improved metabolic status. Adiponectin concentrations were higher in Adipoq-Tst mice than in nontransgenic littermate controls (**Fig. 3a**), consistent with elevated hepatic fat oxidation and an antidiabetic phenotype[25]. As compared to C57BL/6N mice, Adipoq-Tst mice showed mildly improved glucose homeostasis when fed a control diet (**Supplementary Fig. 5a**,**b**), and they were markedly protected from impaired glucose homeostasis after 6 weeks on a HFD (**Supplementary Fig. 5c**,**d**). In support of the idea of preserved metabolic health, even before body-weight differences became apparent (**Fig. 2d**), euglycemic clamp experiments revealed greater whole-body insulin sensitivity (**Fig. 3b** and **Supplementary Table 3**) and glucose uptake in the muscle and adipose tissue of Adipoq-Tst mice (**Fig. 3c**), as compared to those in C57BL/6N mice, after 2 weeks on a HFD. Adipose tissue from Adipoq-Tst mice had higher levels of solute carrier family (facilitated glucose transporter), member 4 (*Slc2a4*; also known as *Glut4*) mRNA (**Supplementary Fig. 5e**) and GLUT4 protein (**Fig. 3d**),

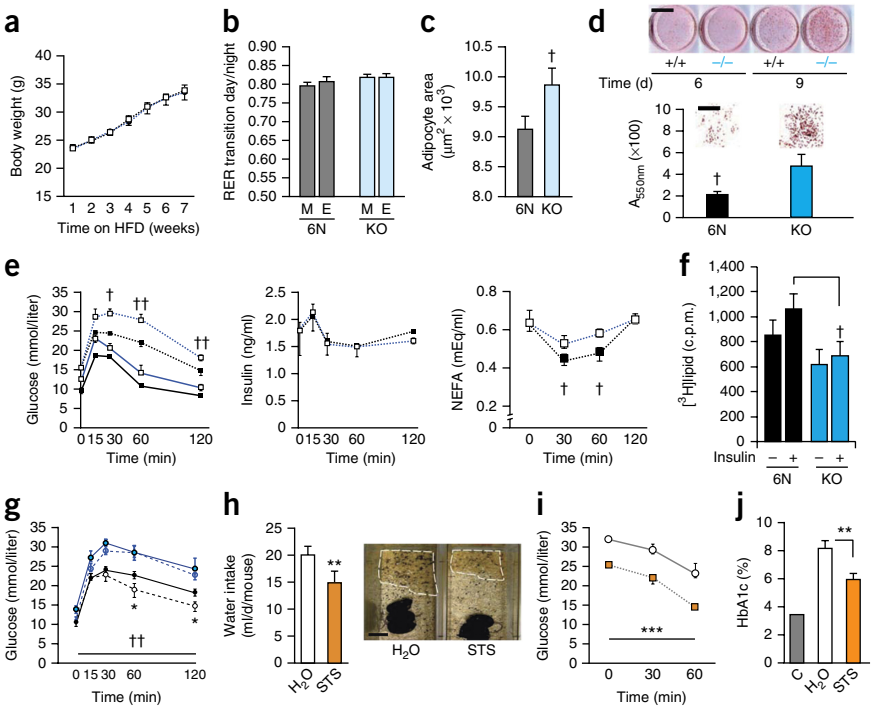

Figure 4 The effects of *Tst* gene knockout and TST activation on diabetes in mice. (**a**) Weight gain in C57BL/6N (squares, $n = 6$) and $Tst^{-/-}$ mice (circles, $n = 5$) during 6 weeks on a HFD. (**b**) Mean morning (M) and evening (E) respiratory exchange ratio (RER) in C57BL/6N ($n = 6$) and $Tst^{-/-}$ ($n = 5$) mice after 6 weeks on a HFD (**b**). (**c**) Adipocyte size in C57BL/6N ($n = 4$) or $Tst^{-/-}$ ($n = 5$) mice after 6 weeks on a HFD. $^{\dagger}P < 0.05$ by Student's *t*-test. (**d**) Representative images for lipid staining at days 6 and 9 of differentiation (top) and quantification of lipids on day 9 (bottom) in SVFs from C57BL/6N (+/+ or 6N; $n = 6$) or $Tst^{-/-}$ (−/− or KO; $n = 5$) mice. Scale bar, 25 mm. Insets, day 9 SVFs at higher magnification. Scale bars, 500 μm (top), 25 mm (insets). $^{\dagger}P < 0.05$ by Student's *t*-test. (**e**) Glucose tolerance (left), insulin excursion (middle) and NEFA excursion (right) in C57BL/6N mice (black lines) or $Tst^{-/-}$ mice (blue lines) fed a control diet (solid lines; 6N, $n = 4$; $Tst^{-/-}$, $n = 5$) or a HFD (broken lines; $n = 5$ per genotype) for 6 weeks. $^{\dagger}P < 0.05$ and $^{\dagger\dagger}P < 0.01$ by RM ANOVA (HFD). (**f**) [^{3}H]glucose incorporation into lipid in adipocytes from C57BL/6N or $Tst^{-/-}$ mice treated without or with insulin ($n = 11$ mice per group). $^{\dagger}P < 0.05$ by two-way ANOVA. (**g**) Glucose tolerance in HFD-fed C57BL/6N (black lines) or $Tst^{-/-}$ mice (blue lines) after 6 weeks of water (solid lines) or thiosulfate (broken lines) administration ($n = 6$ mice per group). $^{\dagger\dagger}P < 0.01$ and $^{*}P < 0.05$ by two-way ANOVA. (**h**) Quantification of water intake (left) and illustrative images of urine output in the cages (right) of C57BL/KsJ-$Lepr^{db/db}$ mice administered water (H_2O; $n = 5$) or thiosulfate (STS; $n = 6$). Scale bar, 5 cm. (**i**,**j**) insulin tolerance (**i**) and glycosylated hemoglobin (HbA1c) levels (**j**) in C57BL/KsJ-$Lepr^{db/db}$ mice treated with water (white bars or circles; $n = 5$) or thiosulfate (orange bar or squares; $n = 6$). C indicates reference C57BL/6J HbA1c values ($n = 2$). In **g**–**j**, $^{*}P < 0.05$, $^{**}P < 0.01$, $^{***}P < 0.001$ by Student's *t*-test (**h**,**j**) or RM ANOVA (**g**,**i**); $^{\dagger\dagger}P < 0.01$ by RM ANOVA (**g**). Throughout, data are mean ± s.e.m.

an important insulin-regulated facilitative glucose transporter. This supported the idea of insulin sensitization in primary adipose tissue as key to whole-body insulin sensitization[26]. In further support of this hypothesis, we found reduced levels of phosphorylated protein kinase B (pAKT) in the adipose tissue of C57BL/6N littermates but not in that of Adipoq-Tst mice that were on a HFD for 6 weeks (**Fig. 3e**). Additionally, we observed that endogenous insulin suppressed free fatty acid (NEFA) release to a greater extent in Adipoq-Tst mice *in vivo* (**Supplementary Fig. 5f**). Indices of lipolytic capacity (such as mRNA levels of adrenergic receptor, beta 3 (*Adrb3*)) were suppressed by a HFD in C57BL/6N littermates but not in Adipoq-Tst mice (**Fig. 3f**). Indeed, Adipoq-Tst mice that were maintained on a HFD showed basally lower amounts of phosphorylated hormone-sensitive lipase (HSL; encoded by *Lipe*; antibody detects phosphorylation on Ser660), whereas C57BL/6N littermates showed a distinct suppression of $pHSL^{S660}$ levels after 6 weeks on a HFD (**Fig. 3g**). We found a selective reduction in levels of the key triglyceride lipase patatin-like phospholipase domain containing 2 (PNPLA2; also known as ATGL)) in the adipose tissue of Adipoq-Tst mice but not in the adipose tissue of control mice that were on a HFD (**Fig. 3h**). We observed a similar response for peripilin 1 (PLIN1) in HFD-fed C57BL/6N and Adipoq-Tst mice (**Supplementary Fig. 5g**). To directly test whether lipolytic capacity was altered *in vivo*, we administered the β3 agonist CL316,243 (CL) to both groups of mice and found that Adipoq-Tst mice had enhanced NEFA release (**Fig. 3i**). Furthermore, adipocytes from Adipoq-Tst mice (basal, Adipoq-Tst versus C57BL/6N: 16 ± 4 versus 27 ± 3 pmol per min per 10^3 adipocytes, respectively; $n = 6$ mice per group) showed enhanced responsiveness to CL treatment (Adipoq-Tst versus C57BL/6N: +171 ± 20 versus +141 ± 13 pmol per min per 10^3 adipocytes, respectively; $n = 6$ mice per group; $P < 0.01$) and pronounced suppression of CL-induced lipolysis in response to treatment with 0.5 nM insulin (CL + insulin, Adipoq-Tst versus C57BL/6N: −126 ± 16 versus −82 ± 8 pmol per min per 10^3 adipocytes; $n = 6$ mice per group; $P < 0.01$, data are mean ± s.e.m., by two-way analysis of variance (ANOVA)) *in vitro*.

Tst deficiency and TST activation have reciprocal metabolic effects

We then determined whether loss of *Tst* gene function, as shown by a complete loss of TST enzyme activity (**Supplementary Fig. 5h**), was causal for obesity or diabetes. After 6 weeks on a HFD, $Tst^{-/-}$ mice had comparable gross body weight, energy expenditure and fat mass to C57BL/6N littermates (**Fig. 4a**,**b** and **Supplementary Fig. 5i**). Nevertheless, histologically, HFD-fed $Tst^{-/-}$ mice showed mild adipocyte hypertrophy *in vivo* (**Fig. 4c**). To explore this further, we differentiated adipose stromal vascular cells (SVFs) *in vitro* and found that SVFs from $Tst^{-/-}$ mice had greater amounts of late-stage lipid accumulation than SVFs from C57BL/6N mice (day 9; **Fig. 4d**), coincident with *Tst* expression in late adipogenesis (**Fig. 2a**,**b**). Transcriptional regulators of early preadipocyte differentiation were comparable between SVFs from mice of the different genotypes (**Supplementary Fig. 5j**). Despite comparable adiposity glucose intolerance was observed in $Tst^{-/-}$ mice, and this was exacerbated with a HFD as compared to that in C57BL/6N mice (**Fig. 4e**). The glucose tolerance test (GTT) also revealed impaired NEFA suppression in $Tst^{-/-}$ mice on a HFD, as compared to that in C57BL/6N mice, despite comparable endogenous insulin output (**Fig. 4e**), an indicator of adipose insulin resistance that was confirmed in primary adipocytes from $Tst^{-/-}$ mice *in vitro* (**Fig. 4f**).

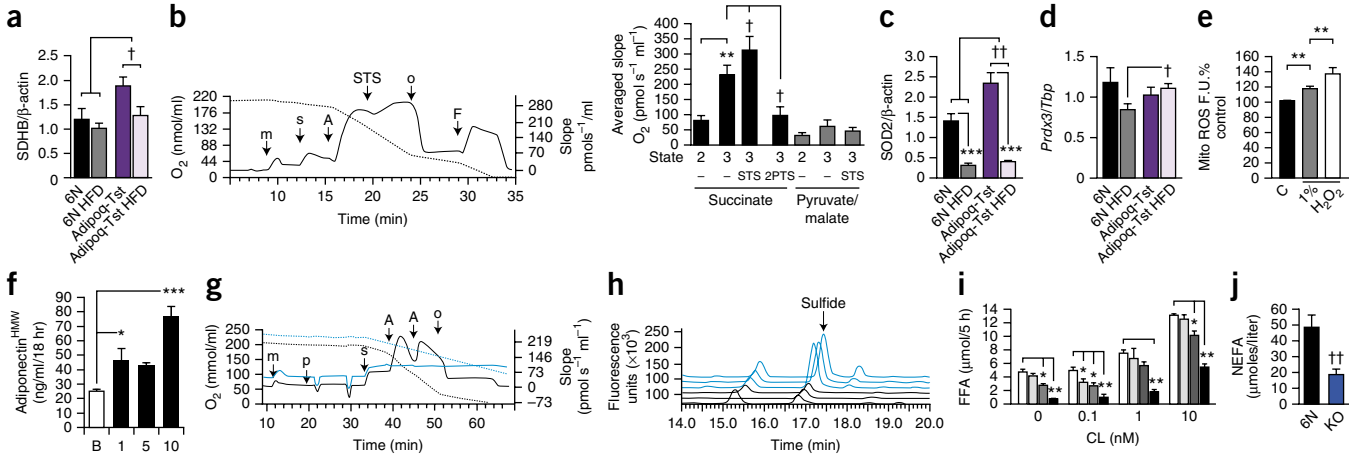

Figure 5 TST beneficially modulates mitochondrial functions. (**a**) SDHB levels, as determined by western blot analysis, in C57BL/6N and Adipoq-Tst mice fed a control diet (6N, $n = 5$; Adipoq-Tst, $n = 5$) or a HFD (6N HFD, $n = 6$; Adipoq-Tst HFD, $n = 6$) for 6 weeks. $^{\dagger}P < 0.05$ (effect of genotype) by two-way ANOVA. (**b**) Left, representative respiration trace for mitochondria (m) plus succinate (s), ADP (A), thiosulfate (STS), the ATP synthase inhibitor oligomycin (o) and uncoupler FCCP (F) (left) in mitochondria from wild-type mice fed a control diet. Dashed line, oxygen concentration; black solid line, rate of change of oxygen (referred to as the slope). Right, average slope of respiration of succinate, or of pyruvate and malate, ± ADP, STS or 2-PTS ($n = 3$ independent experiments). State 2, substrate-only respiration; State 3, respiration with substrate and ADP. $^{**}P < 0.01$ and $^{\dagger}P < 0.05$ by one-way ANOVA. (**c**) Superoxide dismutase (SOD2) protein levels in mice treated as in **a** (6N, $n = 5$; Adipoq-Tst, $n = 5$; 6N HFD, $n = 6$; Adipoq-Tst HFD, $n = 6$). (**d**) Peroxiredoxin-3 (*Prdx3*) mRNA levels in groups as described in **a** (6N, $n = 5$; Adipoq-Tst, $n = 5$; 6N HFD, $n = 3$; Adipoq-Tst HFD, $n = 5$). For **c**,**d**, $^{***}P < 0.001$, $^{\dagger}P < 0.05$ and $^{\dagger\dagger}P < 0.01$ by two-way ANOVA. (**e**) Mitochondrial ROS in control (C; $n = 22$), shRNAmir-treated (gray bar, $n = 14$) or shRNA*Tst*mir-treated (white bar, $n = 8$) 3T3-L1 adipocytes. $^{**}P < 0.01$ by one-way ANOVA. (**f**) Adiponectin secretion from 3T3-L1 adipocytes treated with STS (0–10 mM) ($n = 4$ replicates per condition). B indicates basal secretion without STS treatment. $^{*}P < 0.05$ and $^{***}P < 0.001$ by one-way ANOVA. (**g**) Sulfide effects on mitochondrial respiration from C57BL/6N (black lines) or *Tst*$^{-/-}$ (blue lines) mice. Axes as in **b**, with 'p' indicating the time at which rotenone, pyruvate and malate were added to modulate complex I (representative trace of $n = 3$ independent experiments). (**h**) Blood sulfide levels in C57BL/6N (black lines) or *Tst*$^{-/-}$ (blue lines) mice. Lines represent traces from individual mice ($n = 3$ mice per group). (**i**) Sulfide (0–500 μM) effects on NEFA release from 3T3-L1 adipocytes exposed to CL316,243 (0.1–10.0 nM). $^{*}P < 0.05$ and $^{**}P < 0.01$ (effect of sulfide) by ANOVA. CL effects omitted for clarity. (**j**) NEFA release from adipocytes of C57BL/6N (black bar) or *Tst*$^{-/-}$ (blue bar) mice ($n = 3$ mice per group)). $^{\dagger\dagger}P < 0.01$ by Student's *t*-test. Throughout, quantitative data are mean ± s.e.m.

Therapeutic potential was assessed by treatment with the TST substrate thiosulfate[10,27], which ameliorated HFD-induced glucose intolerance in C57BL/6N, but not *Tst*$^{-/-}$, mice (**Fig. 4g**) and modestly reduced weight gain without altered fecal fat excretion (**Supplementary Fig. 6a**,**d**). We then showed that thiosulfate treatment markedly ameliorated the existing polydipsia, polyuria (**Fig. 4h**), insulin-resistance (**Fig. 4i**; glucose decrement at 60 min as a percentage of the 30-min value after 2 mU per g body weight (mU/g) humulin S: water-treated, −21 ± 4%; thiosulfate-treated, −35 ± 4%; $P < 0.05$ by *t*-test) and an elevated glycosylated hemoglobin A1c content (%HbA1c) in C57BL/KsJ-*Lep*$^{db/db}$ mice with diabetes (**Fig. 4j**), but treatment with thiosulfate did not alter body weight or fat mass (**Supplementary Fig. 6e**,**f**).

TST affects multiple mitochondrial pathways

We next sought evidence for mitochondrial processes that could support a beneficial metabolic effect of elevated amounts of TST (**Fig. 1c**). Adipose tissue from Adipoq-Tst mice had higher protein levels for the iron–sulfur (Fe-S)-containing succinate dehydrogenase (SDH) B subunit (**Supplementary Fig. 7a**). Higher amounts of SDHB protein were maintained in the adipose tissue of Adipoq-Tst mice but not C57BL/6N mice that were on a HFD (**Fig. 5a**). Mitochondrial aconitase 2 (ACO2) and cytosolic ACO1 (**Supplementary Fig. 7a–c**) levels were comparable between the adipose tissues of Adipoq-Tst and C57BL/6N littermates. Thiosulfate was not a mitochondrial substrate *per se* (**Supplementary Fig. 7d**), and it tended to suppress pyruvate and malate (complex I, NADH dehydrogenase) metabolism but augment succinate metabolism (**Fig. 5b**). In contrast, treatment with the TST inhibitor 2-propenyl thiosulfate (2-PTS)[28] abolished succinate metabolism (**Fig. 5b**).

We found that, for mice on a HFD, protein levels of mitochondrial superoxide dismutase 2 (SOD2) and mRNA levels of peroxiredoxin 3 (*Prdx3*) were higher in adipose tissue from Adipoq-Tst mice than in adipose tissue from C57BL/6N littermates (**Fig. 5c**,**d**), with no difference in the amount of cytosolic SOD1 (**Supplementary Fig. 7e**), which was indicative of TST interactions with mitochondrial reactive oxygen species (ROS). In support of a functional role of TST on ROS, knockdown of *Tst* (using a lentiviral-encoded *Tst*-specific shRNA) (**Supplementary Fig. 7f**) engendered higher levels of mitochondrial ROS after cells were exposed to oxidative stress (**Fig. 5e**). Moreover, ROS-sensitive[17,19,29] adiponectin release from 3T3-L1 adipocytes was reduced by inhibition of TST activity with 2-PTS treatment (**Supplementary Fig. 7g**) (basal versus 10 μM 2-PTS treatment: 40 ± 1 ng/ml versus 25 ± 1 ng/ml, respectively; $n = 3$ replicates; $P < 0.01$), whereas adiponectin release was increased after treatment with thiosulfate (**Fig. 5f**). Finally, a functional role for TST in H_2S metabolism was established because isolated mitochondria from *Tst*$^{-/-}$ mice showed greater sensitivity to sulfide-mediated suppression of succinate respiration (**Fig. 5g**) and because blood sulfide levels were markedly higher in *Tst*$^{-/-}$ than in C57BL/6N mice *in vivo* (**Fig. 5h**). Dose-dependent sulfide suppression of 3T3-L1 adipocyte lipolysis (**Fig. 5i**) and reduced basal lipolysis in adipocytes from *Tst*$^{-/-}$ mice *in vitro* (**Fig. 5j**) supported a role for TST modulation of H_2S effects on adipocyte function.

Parallels for TST biology in humans

In support of a conservation of function for TST in humans, we found that levels of *TST* mRNA were higher in adipose tissue from lean subjects than in adipose tissue from subjects who were obese (**Fig. 6a**)

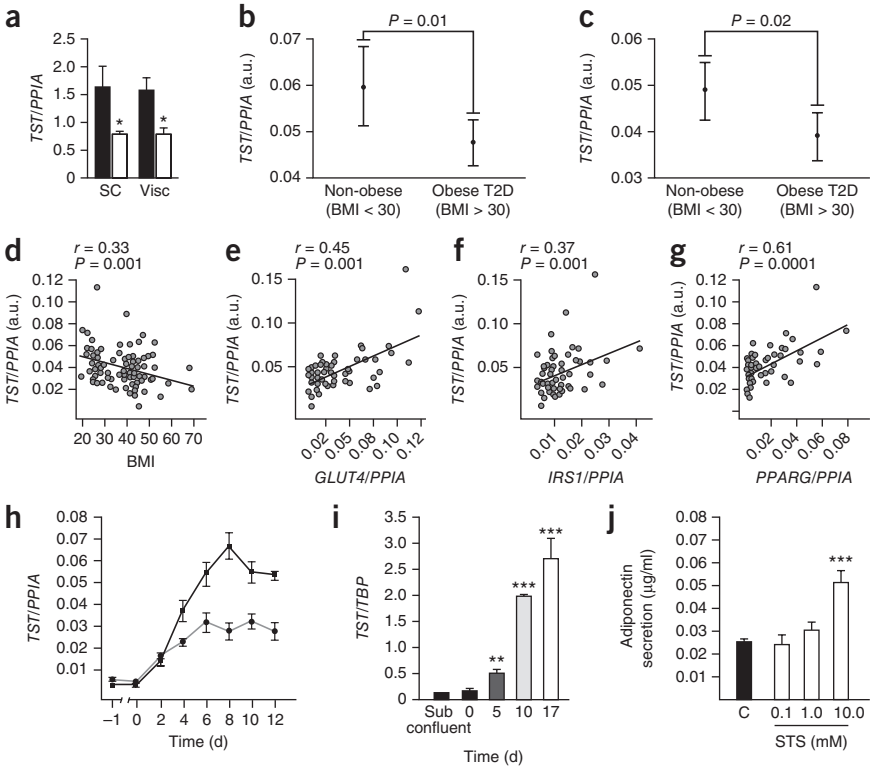

Figure 6 *TST* mRNA levels in human adipose tissue correlate with insulin sensitivity. (**a**) *TST* mRNA levels in human subcutaneous (SC) and visceral (Visc) adipose tissue from lean (black bars) and obese (white bars) women from a Viennese cohort ($n = 8$ subjects per group). $^*P < 0.05$ by two-way ANOVA. (**b**,**c**) *TST* mRNA levels in subcutaneous (**b**) and visceral (**c**) adipose tissue from subjects of a Spanish case-control cohort[31] who are either non-obese ($n = 28$) or obese with type 2 diabetes (T2D) ($n = 22$ (**b**) or $n = 23$ (**c**)). a.u., arbitrary units. (**d**–**g**) Correlations of *TST* mRNA levels in adipose tissue with body mass index (BMI; $n = 96$) (**d**) or with mRNA levels for markers of adipose insulin sensitivity, including *GLUT4* ($n = 58$) (**e**), *IRS1* ($n = 71$) (**f**) and *PPARG* ($n = 59$) (**g**). *PPIA*, peptidylprolyl isomerase A. (**h**,**i**) *TST* mRNA levels in differentiating primary human subcutaneous (black line) and omental (gray line) preadipocytes (**h**) and in clonal human SGBS adipocytes (**i**) ($n = 6$ replicates per time point). $^{**}P < 0.01$ and $^{***}P < 0.001$ (relative to day 0 values) by one-way ANOVA. (**j**) The effects of 6 h of STS treatment (0.1–10.0 mM) on adiponectin secretion from differentiated human SGBS adipocytes ($n = 4$ replicates). $^{***}P < 0.001$ (relative to control (C)) by ANOVA. In **a**–**c**, **h**–**j**, data are mean ± s.e.m. Significance of correlational data for *TST* and other adipose genes was assessed with Scheffé *post hoc* tests.

in a population of Austrian individuals. Furthermore, *TST* mRNA levels in the subcutaneous adipose tissue from a large sample ($n = 673$) of Icelandic individuals[30] correlated negatively with body mass index (BMI; $r = -0.249$, $P = 1.7 \times 10^{-10}$). Moreover, in a Spanish cohort[31], the adipose tissue of subjects who were obese and had type 2 diabetes (T2D) had lower levels of *TST* mRNA than subjects who were not obese and who did not have T2D; *TST* mRNA levels thus correlated negatively with BMI (**Fig. 6b–d** and **Supplementary Table 4**). *TST* mRNA levels in adipose tissue correlated positively with levels of *GLUT4*, insulin substrate receptor 1 (*IRS1*) and peroxisome proliferator activated receptor gamma (*PPARG*) mRNA (**Fig. 6e–g** and **Supplementary Table 4**), independently of BMI after adjusting with multivariate linear regression (*GLUT4*, $P < 0.001$; *IRS1*, $P < 0.006$; *PPARG*, $P < 0.001$). *TST* mRNA levels also correlated with markers of lipolytic capacity and lipid droplet formation (**Supplementary Fig. 8**).

The *TST* mRNA levels were higher in differentiated human primary fat cells (**Fig. 6h**) and in differentiated human SGBS[32] clonal adipocytes than in preadipocytes (**Fig. 6i**). Similarly to that observed with rodent adipocytes (**Fig. 5f**), thiosulfate treatment increased adiponectin release from human SGBS adipocytes (**Fig. 6j**).

DISCUSSION

Genetic mechanisms that maintain metabolic health and counter excess adiposity have received less attention than those associated with obesity. One example is polymorphisms at the *MC4R* locus that are associated with protection against obesity[33]. *MC4R* variants reflected a generality borne from early-obesity genome-wide association studies (GWAS) that emphasize the predominance of brain-regulated appetite and energy expenditure pathways in explaining adiposity levels in the population[33–35]. Later GWAS that used techniques to more accurately measure fat mass, such as dual energy X-ray absorptiometry (DEXA), revealed a new class of genes with direct functions in the adipose tissue[35,36]. Variation at the *IRS1* locus[35–37] revealed an adipose mechanism that linked reduced peripheral fat deposition with impaired metabolic health[35]. From this we hypothesized the existence of adipose-specific mechanisms driving obesity resistance. However, dedicated GWAS in extremely lean, but healthy, humans that targets a population distinct from those with lipodystrophy[38] or failure-to-thrive[39] syndromes had not been reported. To gain insight into this elusive genetic category of healthy lean individuals and to focus on mechanisms in adipose tissues, we exploited the polygenic lean line of mice[4–8,22]. Polygenic lean and fat lines resemble the genetic architecture of common human adiposity and do not derive from single adiposity genes with very large effect sizes[4–8] (such as leptin[40]), thereby improving our chances of finding novel adiposity genes. Moreover, because lean mice were selected for extremely low adiposity but maintained lean mass, they are distinct from models that are selected for obesity studies (relative to a control line) or from those that are selected on overall body weight with adiposity as a correlated trait[41]. This may explain why the M2 sub-sub-congenic effect size is relatively large for a QTL study of a polygenic trait, supporting a prominent role for *Tst* as a causal leanness gene in the lean line of mice.

Compensatory alleles in the obesity-susceptible C57BL/6N genetic background that were chosen to model transgenic adipose *Tst* overexpression may explain the absence of gross baseline leanness in Adipoq-Tst mice. However, the effect size of obesity resistance in HFD-fed Adipoq-Tst transgenic mice supports higher *Tst* levels as an anti-obesity and antidiabetic mechanism. The *Tst* effect size is also large as compared to human adiposity GWAS hits; the fat mass and obesity associated (*FTO*) and iroquois homeobox 3 (*IRX3*)[34] locus has −0.33% body fat per effect allele[35]. Greater genetic and environmental heterogeneity in human populations is a probable explanation for this. Nevertheless, the *Tst* allele effect has allowed us

to identify a novel driver for reduced adiposity and improved metabolic health in lean mice that has functional parallels in other mouse strains and in humans. Conserved regulation across states of adiposity and metabolic health indicate dynamic expression control by varied mechanisms. Furthermore, although common variant human adiposity GWAS have not identified hits at the *TST* locus, we may infer biological significance from our observed parallels in human TST expression and function. The *Tst* effect is a metabolically protective reduction of fat mass across all depots in mice. *TST* mRNA levels are comparable in subcutaneous and visceral fat in humans, suggesting protection in both depots.

Obesity resistance to a HFD does not involve WAT beigeing[42,43] in lean[8] or Adipoq-Tst mice. Indeed, fat mice on a HFD showed WAT beigeing, which failed to prevent exaggerated obesity[8]. Consistent with novel WAT-derived leanness mechanisms in lean mice, beigeing genes (such as *Ppargc1* and *Ucp1*) do not map to the major adiposity QTLs[5,6]. Such alternative mechanisms have a precedent, with some parallels and distinctions, as compared to increases in *Tst* levels. An adipocyte-specific knockout of the gene encoding the mitochondrial transcription factor TFAM (F-TFKO) caused a loss of complex I proteins, a compensatory increase of nuclear-encoded SDH activity and increased adipose and whole-body energy expenditure, without canonical beigeing[17]. Notably, F-TFKO mice showed a confounding increase of mitochondrial ROS with lower adiponectin release[17], whereas elevated TST levels may quench ROS and increase adiponectin levels. In contrast, adipocyte-specific overexpression of the outer mitochondrial membrane iron-transport-inhibiting protein mitoNEET caused pronounced obesity but with elevated adiponectin-associated lipogenic WAT expansion and reduced mitochondrial ROS[19]. TST-mediated leanness presumably derives from altered mitochondrial substrate preference combined with effective ROS and H_2S quenching, which maintains insulin sensitization in adipose tissue, lipolytic responsiveness and adiponectin release that ultimately drives peripheral oxidative disposal of excess fat.

Thiosulfate, a TST activator, is involved in cyanide detoxification[10], and oral thiosulfate administration has been found to ameliorate heart failure in mice[27]. Thiosulfate treatment ameliorated diabetes but did not consistently reduce fat mass, suggesting that TST activation is predominantly involved in an antidiabetic mechanism. This is supported by our findings that transgenic manipulation of *Tst* predominantly affected glucose homeostasis rather than fat mass *per se* and that human TST is associated with metabolic status after adjustment for BMI. An increase in TST protein levels may have broader beneficial effects that are not recapitulated by increasing the availability of a single substrate. It is also possible that thiosulfate efficacy was limited by low oral bioavailability and the additional confounder of low target adipose TST that is found in obese mice. Notably, millimolar concentrations of thiosulfate were needed to elicit beneficial effects *in vitro* and *in vivo*. Similar compound ranges have been noted for other antidiabetic drugs, including salicylate[44] and metformin[45]. The development of TST activators that are more efficacious and have higher specificity is needed to realize the therapeutic potential of this novel antidiabetic target.

METHODS

Methods and any associated references are available in the online version of the paper.

Accession codes. ArrayExpress: microarray data for the fat and lean mice can be found under accession code E-MEXP-3094. Gene Expression Omnibus: the RNA-seq data for the DO mouse livers and the founder strain adipose tissue can be found under accession codes GSE45684 and GSE80162, respectively.

Note: Any Supplementary Information and Source Data files are available in the online version of the paper.

ACKNOWLEDGMENTS

N.M.M. was supported by a Career Development Fellowship, an Institutional Strategic Support Fund award and a New Investigator Award from the Wellcome Trust (100981/Z/13/Z), a Research Councils UK Fellowship and a British Heart Foundation Centre of Research Excellence exchange award. We thank the Slovenian Research Agency for support (core funding P4-0220; project N5-0003 Syntol and J4-6804; all to S.H.) and for a Young Scientist Fellowship (J.B.). We acknowledge support of the British Heart Foundation Research Excellence Award in support of the contribution by the Bioinformatics Core (D.R.D.). T.M.S. received funding from the Federal Ministry of Economy, Family and Youth and from the Austrian National Foundation for Research, Technology and Development. G.A.C. was supported by the US National Institutes of Health grant R01GM 070683. J.M.F.-R. acknowledges funding from FIS PI11/00214. A.V.-P. was funded by the UK Medical Research Council (MRC) MDU, an MRC Programme grant, MRC DMC Core and MITIN (HEALTH-F4-2008-223450). We thank M. Wabitsch (University of Ulm) for the gift of the SGBS human preadipocyte cell line.

AUTHOR CONTRIBUTIONS

N.M.M. and S.H. conceived the experiments; N.M.M., J.B., R.N.C., Z.M., G.G., S.C.M., S.R.-C., C.M., M.E.B.-L., R.E.A., L.R., A.F.H. and S.H. performed experiments on *in vivo* models or samples; N.M.M., R.N.C., J.M.M.-N., M.T.G.G., C.M. and A.G. performed experiments on *in vitro* models; J.M.M.-N., V.G., J.M.F.-R. and V.E. provided and analyzed gene expression data from human adipose tissue; M.Z. and T.M.S. provided human adipose tissues; G.N. generated the TST inhibitor; A.S. and P.S. generated the Adipoq-Tst mice; Z.V.W. generated the adiponectin promoter DNA vector; D.R.D. performed bioinformatics analyses; S.C.M., K.L.S. and G.A.C. generated the Diversity Outbred mouse resources and data; S.R.-C., C.J.K., J.R.S., B.R.W., S.P.W., A.V.-P., J.M.F.-R., V.E. and S.H. discussed results and commented on the manuscript; and N.M.M. and S.H. wrote the paper.

COMPETING FINANCIAL INTERESTS

The authors declare competing financial interests: details are available in the online version of the paper.

1. Flegal, K.M., Carroll, M.D., Ogden, C.L. & Curtin, L.R. Prevalence and trends in obesity among US adults, 1999–2008. *J. Am. Med. Assoc.* **303**, 235–241 (2010).
2. Yanovski, S.Z. & Yanovski, J.A. Obesity prevalence in the United States—up, down or sideways? *N. Engl. J. Med.* **364**, 987–989 (2011).
3. Ljungvall, A. & Zimmerman, F.J. Bigger bodies: long-term trends and disparities in obesity and body-mass index among U.S. adults, 1960–2008. *Soc. Sci. Med.* **75**, 109–119 (2012).
4. Morton, N.M. *et al.* A polygenic model of the metabolic syndrome with reduced circulating and intra-adipose glucocorticoid action. *Diabetes* **54**, 3371–3378 (2005).
5. Horvat, S. *et al.* Mapping of obesity QTLs in a cross between mouse lines divergently selected on fat content. *Mamm. Genome* **11**, 2–7 (2000).
6. Prevorsek, Z., Gorjanc, G., Paigen, B. & Horvat, S. Congenic and bioinformatics analyses resolved a major-effect *Fob3b* QTL on mouse chr 15 into two closely linked loci. *Mamm. Genome* **21**, 172–185 (2010).
7. Bünger, L. *et al.* Long-term divergent selection on fatness in mice indicates a regulation system independent of leptin production and reception. *FASEB J.* **17**, 85–87 (2003).
8. Morton, N.M. *et al.* A stratified transcriptomics analysis of polygenic fat and lean mouse adipose tissues identifies novel candidate obesity genes. *PLoS One* **6**, e23944 (2011).
9. Westley, J. Rhodanese. *Adv. Enzymol.* **39**, 327–368 (1973).
10. Hall, A.H., Saiers, J. & Baud, F. Which cyanide antidote? *Crit. Rev. Toxicol.* **39**, 541–552 (2009).
11. Bonomi, F., Pagani, S., Cerletti, P. & Cannella, C. Rhodanese-mediated sulfur transfer to succinate dehydrogenase. *Eur. J. Biochem.* **72**, 17–24 (1977).
12. Pagani, S. & Galante, Y.M. Interaction of rhodanese with mitochondrial NADH dehydrogenase. *Biochim. Biophys. Acta* **742**, 278–284 (1983).
13. Nandi, D.L., Horowitz, P.M. & Westley, J. Rhodanese as a thioredoxin oxidase. *Int. J. Biochem. Cell Biol.* **32**, 465–473 (2000).

14. Wang, R. Physiological implications of hydrogen sulfide: a whiff exploration that blossomed. *Physiol. Rev.* **92**, 791–896 (2012).
15. Tiranti, V. *et al.* Loss of ETHE1, a mitochondrial dioxygenase, causes fatal sulfide toxicity in ethylmalonic encephalopathy. *Nat. Med.* **15**, 200–205 (2009).
16. Smirnov, A. *et al.* Mitochondrial enzyme rhodanese is essential for 5 S ribosomal RNA import into human mitochondria. *J. Biol. Chem.* **285**, 30792–30803 (2010).
17. Vernochet, C. *et al.* Adipose-specific deletion of *Tfam* increases mitochondrial oxidation and protects mice against obesity and insulin resistance. *Cell Metab.* **16**, 765–776 (2012).
18. Tormos, K.V. *et al.* Mitochondrial complex III ROS regulate adipocyte differentiation. *Cell Metab.* **14**, 537–544 (2011).
19. Kusminski, C.M. *et al.* MitoNEET-driven alterations in adipocyte mitochondrial activity reveal a crucial adaptive process that preserves insulin sensitivity in obesity. *Nat. Med.* **18**, 1539–1549 (2012).
20. Geng, B. *et al.* Increase or decrease hydrogen sulfide exert opposite lipolysis but reduce global insulin resistance in high-fat-diet-induced obese mice. *PLoS One* **8**, e73892 (2013).
21. Feng, X. *et al.* Hydrogen sulfide from adipose tissue is a novel insulin resistance regulator. *Biochem. Biophys. Res. Commun.* **380**, 153–159 (2009).
22. Simoncic, M. *et al.* Divergent physical activity and novel alternative responses to high-fat feeding in polygenic fat and lean mice. *Behav. Genet.* **38**, 292–300 (2008).
23. Svenson, K.L. *et al.* High-resolution genetic mapping using the Mouse Diversity outbred population. *Genetics* **190**, 437–447 (2012).
24. Wang, Z.V., Deng, Y., Wang, Q.A., Sun, K. & Scherer, P.E. Identification and characterization of a promoter cassette conferring adipocyte-specific gene expression. *Endocrinology* **151**, 2933–2939 (2010).
25. Xu, A. *et al.* The fat-derived hormone adiponectin alleviates alcoholic and non-alcoholic fatty liver diseases in mice. *J. Clin. Invest.* **112**, 91–100 (2003).
26. Herman, M.A. *et al.* A novel ChREBP isoform in adipose tissue regulates systemic glucose metabolism. *Nature* **484**, 333–338 (2012).
27. Sen, U. *et al.* Cardioprotective role of sodium thiosulfate on chronic heart failure by modulating endogenous H_2S generation. *Pharmacology* **82**, 201–213 (2008).
28. Sabelli, R. *et al.* Rhodanese–thioredoxin system and allyl sulfur compounds. *FEBS J.* **275**, 3884–3899 (2008).
29. Koh, E.H. *et al.* Essential role of mitochondrial function in adiponectin synthesis in adipocytes. *Diabetes* **56**, 2973–2981 (2007).
30. Emilsson, V. *et al.* Genetics of gene expression and its effect on disease. *Nature* **452**, 423–428 (2008).
31. Moreno-Navarrete, J.M. *et al.* Decreased *RB1* mRNA, protein and activity reflect obesity-induced altered adipogenic capacity in human adipose tissue. *Diabetes* **62**, 1923–1931 (2013).
32. Wabitsch, M. *et al.* Characterization of a human preadipocyte cell strain with high capacity for adipose differentiation. *Int. J. Obes. Relat. Metab. Disord.* **25**, 8–15 (2001).
33. Loos, R.J. The genetic epidemiology of melanocortin 4 receptor variants. *Eur. J. Pharmacol.* **660**, 156–164 (2011).
34. Smemo, S. *et al.* Obesity-associated variants within FTO form long-range functional connections with IRX3. *Nature* **507**, 371–375 (2014).
35. Kilpeläinen, T.O. *et al.* Genetic variation near *IRS1* associates with reduced adiposity and an impaired metabolic profile. *Nat. Genet.* **43**, 753–760 (2011).
36. Heid, I.M. *et al.* Meta-analysis identifies 13 new loci associated with waist–hip ratio and reveals sexual dimorphism in the genetic basis of fat distribution. *Nat. Genet.* **42**, 949–960 (2010).
37. Rung, J. *et al.* Genetic variant near *IRS1* is associated with type 2 diabetes, insulin resistance and hyperinsulinemia. *Nat. Genet.* **41**, 1110–1115 (2009).
38. Vigouroux, C., Caron-Debarle, M., Le Dour, C., Magré, J. & Capeau, J. Molecular mechanisms of human lipodystrophies: from adipocyte lipid droplet to oxidative stress and lipotoxicity. *Int. J. Biochem. Cell Biol.* **43**, 862–876 (2011).
39. Jacquemont, S. *et al.* Mirror extreme BMI phenotypes associated with gene dosage at the chromosome 16p11.2 locus. *Nature* **478**, 97–102 (2011).
40. Zhang, Y. *et al.* Positional cloning of the mouse obese gene and its human homolog. *Nature* **372**, 425–432 (1994).
41. Mathes, W.F., Kelly, S.A. & Pomp, D. Advances in comparative genetics: influence of genetics on obesity. *Br. J. Nutr.* **106** (suppl. 1), S1–S10 (2011).
42. Soloveva, V., Graves, R.A., Rasenick, M.M., Spiegelman, B.M. & Ross, S.R. Transgenic mice overexpressing the β1-adrenergic receptor in adipose tissue are resistant to obesity. *Mol. Endocrinol.* **11**, 27–38 (1997).
43. Harms, M. & Seale, P. Brown and beige fat: development, function and therapeutic potential. *Nat. Med.* **19**, 1252–1263 (2013).
44. Hawley, S.A. *et al.* The ancient drug salicylate directly activates AMP-activated protein kinase. *Science* **336**, 918–922 (2012).
45. Hawley, S.A. *et al.* Use of cells expressing gamma subunit variants to identify diverse mechanisms of AMPK activation. *Cell Metab.* **11**, 554–565 (2010).

ONLINE METHODS

Experimental animals. All experiments were performed according to guidelines set out by the ethical committees of The University of Edinburgh, The University of Cambridge or the University of Ljubljana, and they were carried out within the framework of the Animals (Scientific Procedures) Act (1986) of the United Kingdom Home Office or related laws from the European Union (Slovenia).

In all studies, animals within genotype cohorts were randomly assigned to diet or intervention groups. All animals were maintained in standard housing with 12-h light and 12-h dark cycles (7 a.m. to 7 p.m.) and *ad libitum* access to the appropriate diet. For *in vivo* experiments (for example, GTT, insulin tolerance test (ITT), euglycemic clamps and CL injections), operators and animal handlers were blinded to the data, which was generated by a second individual who was blinded to the treatment regimen until the code was broken. All of the studies, with the exception of the F_2 crosses of the M and M2 lines with the parental F lines and the RNA-seq analyses of adipose tissue from founder strains (described below), exclusively used male mice to avoid confounding effects of the female hormonal cycle. Male C57BL/6J, C57BL/6N (also referred to as 6N), C57BL/6J$^{lep/lep}$ (Lep^{ob}, 10 weeks old) and C57BL/Ksj$^{lepr/lepr}$ (~8 weeks old) were purchased from certified distributors (Charles River Laboratories or Harlan (UK)). C57BL/Ksj$^{lepr/lepr}$ mice were housed in groups of three and were subsequently housed individually 3 d before ITT was performed, to determine water intake by weighing the water bottle daily and using the result from the third day as representative of stable intake. $Tst^{-/-}$ mice were generated by the University of California at Davis (UCD) knockout-mouse project (https://www.komp.org/geneinfo.php?geneid=85272; project VG13928; model Tst$^{tm1(KOMP)Vlcg}$, representing a definitive null allele). Sperm from viable heterozygote mice were used to fertilize C57BL/6N embryos at the University of Edinburgh Genetic Intervention and Screening technologies (GIST) facility. $Tst^{-/-}$ mice and age-matched littermate controls were placed on experimental diets at approximately 5–6 weeks of age. Adipoq-Tst mice were generated by cloning the mouse *Tst* cDNA downstream of the adiponectin promoter[24] and micro-injecting the construct into C57BL/6J blastocysts by using standard cloning techniques (University of Turku, Finland). In general, Adipoq-Tst and age-matched control littermate mice were placed on experimental diets at approximately 5–6 weeks of age.

High-fat diets (D12331, Research Diets, New Brunswick, US) and either control low-fat high-cornstarch diets (D12328) or standard control chow were used throughout the studies.

The following studies had specific subject exclusion. In the thiosulfate treatment study, one C57BL/Ksj$^{lepr/lepr}$ mouse that was assigned to the control (water) group rapidly and inexplicably lost weight and was humanely culled. All of the data for this mouse were removed from the study. In the euglycemic clamp studies, one animal from each genotype (6N and Adipoq-Tst) failed to recover to pre-operation body weights, and their data was excluded from the study. In one of the high-fat diet cohorts (**Fig. 2e**) comparing 6N to Adipoq-Tst mice (for organ weights), a 6N control mouse failed to gain any weight and was culled due to ill-health during the study. In the gene expression and western blot analyses reported in **Figures 2e–h** and **5d**, prior sample analysis limited available group sizes to below the optimal $n = 6$ for some targets.

Fat (F) and lean (L) polygenic mouse lines. The long-term selection and further development of the F, L and congenic lines are described elsewhere[5,6]. Animals were fed a pelleted diet (Special Diets Services, Witham, Essex, UK) or a defined low- (11% calories as fat with sucrose; D12329) or high-fat (58% calories as fat with sucrose; D12331) diet (Research Diets, New Brunswick, New Jersey).

Experiments using the congenic mouse lines. *Polygenic mouse models*: from a previous F_2 cross[6] a recombinant individual within the *Fob3b* QTL region was used as a founder for the development of the subcongenic line M used here. A total of 11 or 12 backcrosses to the fat line, with additional marker-assisted elimination of other QTL regions, were performed. An F_2 cross between mice of the fat line and the congenic line M was developed and phenotyped ($M \times F_2$ cross). Within this $M \times F_2$ cross (**Supplementary Table 1**), another recombinant individual within the *Fob3b2* QTL region was identified which carried a smaller donor segment from the lean mouse line (**Supplementary Fig. 1**); this recombinant was a founder for the development of the sub-subcongenic line M2, and a subsequent F_2 cross of this mouse with mice from the fat line ($M2 \times F_2$ cross). Positions of the lean mouse donor segments in the congenic lines were defined based on high-density single-nucleotide polymorphism (SNP) genotyping (**Supplementary Fig. 1**). For all experiments, food chow (1324 maintenance diet, Altromin, Germany) and acidified water were offered *ad libitum*, except for mice of the $M2 \times F_2$ cross, in which a high-fat diet (HFD; Research Diets, USA, D12108) was used. 3-week-old $M2 \times F_2$ mice were adjusted to the HFD for 2 weeks and were maintained on it for additional 11 weeks. All of the procedures involving animals were performed according to local ethical and regulatory guidelines, which are all in compliance with the EU regulations regarding research on experimental animals (project license number 34401-3/2007/4). All of the mice were weaned at 3 weeks of age and were group-housed (four mice per cage) in individual ventilated cages (Techniplast Inc., Italy) in a controlled environment (temperature 21 °C, humidity 40–70%, and a 12-h light and 12-h dark cycle). Body weights were recorded at 3, 5, 6, 8, 10, 12, 14 and 16 weeks, at which point the adipose depots—abdominal (Abd), gonadal (epididymal, Epi), subcutaneous–femoral (SC) and mesenteric (MES)—were dissected. The sum of all of the weights of the collected fat depots was used to calculate the adiposity index (ADI).

Empirical distributions of collected phenotypic data suggested a normal distribution for each analyzed variable. Therefore, a statistical model (equation (1)) with multivariate normal distribution was fitted:

$$y \mid b, s, R \sim MVN(X_b + Z_s, R), \tag{1}$$

where y is an $ny \times 5$ matrix of phenotypic values (y) for n mice, b is the vector of location parameters for effects that differed between the data sets, s is the vector of location parameters for n_s seasons of dissection defined as year–month interaction, and $R = I_{ny} \times R_0$ is residual covariance matrix . For F_2 congenic intercrosses ('$M \times F_2$' and '$M2 \times F_2$'), the vector b involved the effect of sex (males and females), parity (1, 2, and 3+), the number of pups per litter (1 or 2, or 3, 4, 5, 6 and 7+), line (M and M2), and genotype within line (homozygotes fat/fat, fat/M and M/M, and heterozygotes fat/M or fat/M2). For the latter, the additive and dominance effect was tested using the deviance information criterion (DIC) statistic, which revealed that the dominance model had a better fit than the additive model. Posterior distributions were summarized with mean and s.d. for each line or genotype, as evaluated at the first parity and five pups in the litter. Posterior probabilities that the congenic lines or homozygous genotypes from F_2 congenic intercrosses differ were computed. High probability, for example, 0.95, would suggest a significant difference and presence of a *Fob3b2* QTL effect.

Bioinformatics analysis of candidate genes in the *Fob3b2* interval. Haplotype analysis was performed to identify haplotype blocks that are not identical by descent (non-IBD) (**Supplementary Fig. 2**). These regions are likely to carry the causal polymorphism(s) that are responsible for the observed phenotypic difference between the three genotypic classes of congenic F_2 progeny. Comparative genomic analyses within the *Fob3b2* region were performed in humans (http://www.genome.gov/gwastudies/), cattle, pigs and chickens (http://www.genome.gov/gwastudies/). If a QTL that was associated with adiposity traits was found to overlap with a *Fob3b2 Tst*-containing region, then it was considered to be a hit. A set of 1,980 SNPs (JAX SNP IDs JAX00405958–JAX00407532) that were located within the *Fob3b2* congenic region of the M line was used to genotype the F, L and congenic M or M2 lines. Interval-specific haplotype analysis was performed to identify haplotype blocks that were not identical by descent (non-IBD) between congenic lines. Such regions are likely to contain the causal polymorphism(s) that cause differences in phenotype between the observed lines[6]. 20 genes mapped to non-IBD regions (see section 'Custom RT–PCR array' below). A tool within the Mouse Phenome database (SNP Wizard) was used for SNP–strain comparisons. By using the Bio GPS Expression database (http://biogps.org), genes were selected based on their expression levels in metabolic tissues in two independent microarray platforms (Affymetrix probe sets MOE430 and GNF1M). If a positional candidate gene showed an expression level three times above the median expression level in at least one of the metabolic tissues (pituitary, brain, white and brown adipose, liver, muscle, intestines stomach, pancreas or adrenal gland), then this was considered to be a hit. Molecular function annotations for the non-IBD candidates were retrieved from the Gene Ontology

doi:10.1038/nm.4115

(GO, http://amigo.geneontology.org) database; any function that could be connected to adipose tissue biology and/or growth was considered a hit. Candidate genes were also queried for any impact on body weight, obesity, food intake or metabolism phenotypes of the knockout and transgenic models using the Mouse Genome Informatics (MGI) database (http://www.informatics.jax.org). Differential expression of all positional non-IBD candidates was verified by using two microarrays—a whole-genome expression Affymetrix Genechip 2.0 array and an Affymetrix Exon chip array—and various tissues from the F and L line mice (ref. 8 and this study (for M2 × F2 microarray)), using expression differences of ≥2-fold. Genes with the largest number of bioinformatics hits (highest-priority candidates) were also separately assayed by qRT–PCR, using the WAT of F, L and M2 line mice. The expression of all positional candidate genes within the core non-IBD region was measured in WAT using custom RT–PCR arrays (Life Technologies); details are in the section 'Custom RT–PCR array analysis' below.

Custom RT–PCR array analysis of positional candidates in the *Fob3b2* segment. The expression of all positional candidate genes within the core non-IBD region was measured in WAT using custom RT–PCR arrays (Life Technologies) comparing homozygotes from the F_2 cross between mice of the M2 and fat lines. All TaqMan assays were custom ordered from Applied Biosystems (assay IDs below). Real-time PCR was performed using a standard TaqMan PCR kit protocol on an Applied Biosystems ViiA 7 Real-time PCR System. The 10-µl PCR reaction included 2 µl cDNA sample, 2× TaqMan Universal Master Mix II, 20× TaqMan Gene Expression Assay Buffer and RNase-free water. The reactions were incubated in a 384-well plate at 50 °C for 2 min, followed by polymerase activation at 95 °C for 10 min, and 40 cycles of 95 °C for 15 s and 60 °C for 1 min each. All reactions, including a no-template control, were run in duplicate. For each sample, the average C_q was calculated and, by normalizing using three endogenous controls (*Actb*, *Tbp* and *Gapdh*), ΔC_q was determined. The $2^{-\Delta\Delta Cq}$ method was used to quantify the relative change in expression of the target group (homozygous for genotype lean/lean in the *Fob3b2* segment). Student's *t*-test analysis was performed, and differential expression of a gene between the F2 homozygote carrying two fat-line-derived alleles and homozygotes carrying two lean-line alleles was considered a hit. Probes used in the study were (gene, assay ID): *Actb*, Mm00607939_s1; *Gapdh*, Mm99999915_g1; *Tbp,* Mm00446971_m1; *Arhgap39*, Mm01197504_m1; *Zfp251*, Mm02342310_m1; *Zfp7*, Mm00524080_m1; *Mb*, Mm00442968_m1; *Apol6*, Mm03990658_m1; *Rbm9*, Mm00612735_m1; *Apol7a*, Mm01200950_m1; *Apol9a*, Mm04206749_gH; *Apol7b*, Mm01616698_m1; *Apol10a*, Mm04214065_g1; *Apol7c*, Mm01628124_s1; *Apol10b*, Mm04212537_m1; *Apol7e*, Mm01616699_m1; *Myh9*, Mm01197036_m1; *Pvalb*, Mm00443100_m1; *Ncf4*, Mm00476300_m1; *Csf2rb2*, Mm00655763_m1; *Csf2rb*, Mm00655745_m1; *Tst*, Mm01195231_m1; and *Mpst*, Mm00460389_m1.

Quantification of allelic *Tst* mRNA expression. To examine whether the *Tst* allele from the lean (L) line is expressed at a higher level than that from the fat (F) line in heterozygote mice from the M2 × F_2 congenic cross, allele-specific TaqMan probes were designed at the SNP in the 3′ UTR (rs31534689). Sequences of the PCR primers were 5′-CCTGCTGTAGGTTCACCTTTTAGG-3′ (forward) and 5′-GGAGGCACCAAGAGCAATTCTAAA-3′ (reverse), and the TaqMan probes at the SNP site (underlined) were CCCTGTCAATCTCCGT (lean-allele specific) ACCCTGTCAATATCCGT (fat-allele specific). To determine the calibration curve, genomic DNA was isolated from two individuals homozygous for genotype FF and LL in the *Fob3b2* segment and mixed in various molar ratios of F allele/L allele using fluorescently labeled probes with VIC fluorescent dye (http://www.genelink.com/newsite/products/mod_detail.asp?modid=63) and 6-fluorescein phosphoramidite (FAM) (VIC allele/FAM allele and dye-swapped)—8:1, 4:1, 2:1, 1:1, 1:2, 1:4 and 1:8. By calculating the log of ($\Delta Rn_{FAM}/\Delta Rn_{VIC}$) for each mixing ratio, a standard curve, with the linear regression line equation $\log_2(\Delta Rn_{FAM}/\Delta Rn_{VIC}) = a + b \times \log_2(_{VIC}\text{allele}/_{FAM}\text{allele})$, was generated. Allele-specific expression of the gene was measured on isolated RNA samples from eight heterozygotes with genetic differences in the *Fob3b2* segment. Through intercepting measured fluorescence intensities on the standard curve, the allele ratio of heterozygous individuals was extrapolated, and the relative expression of lean-line allele:fat-line allele was determined (**Supplementary Fig. 1f,g).**

Correlation analyses between *Tst* expression and other genes or phenotypes. Data sets of gene expression in adipose tissue from different mouse strains were downloaded from BioGPS (http://biogps.org/dataset/8/eqtl-adipose-moe430-v2/), and phenotype data for the same set of strains were obtained from the Mouse Phenome Database (http://phenome.jax.org/; CGDpheno1, 2009). A Pearson's correlation analysis was performed in SAS–STAT software. Strong and highly statistically significant correlations ($P < 0.0001$) between *Tst* and genes expressed in adipose tissue, and between *Tst* and phenotypes, are presented (**Fig. 1e–g**).

RNA sequencing analysis and eQTL mapping. Methods for RNA-seq library preparation, analysis and eQTL mapping in Diversity Outbred (DO) mice have been described in detail[46]. Briefly, liver or inguinal fat pad adipose tissue was dissected from 26-week-old DO or founder strain mice and stored in RNAlater solution (Life Technologies) at −80 °C. Total RNA was extracted using the Trizol Plus RNA extraction kit with on-column DNase digestion (Life Technologies). Indexed mRNA-seq libraries were generated from 1 µg total RNA using the TruSeq kit (Illumina), and 100-bp single-end reads were sequenced on the HiSeq 2000 sequencer (Illumina) according to Illumina protocols. Samples were multiplexed and replicated across 2–4 sequencing lanes to minimize technical variation. Raw RNA-seq fastq files and processed gene-level abundance estimates for the DO liver and founder strain adipose samples are archived at the Gene Expression Omnibus (GEO) database under the accession numbers GSE45684 and GSE80162, respectively. Individualized genome and transcriptome sequences were constructed for every DO and strain sample using Seqnature software[46]. RNA-seq reads were aligned to their respective individualized transcriptomes by using the Bowtie aligner, and gene expression was quantified from the read-alignment profiles using RSEM software as described[46]. Expression quantitative trait loci (eQTLs) in the DO liver samples were identified with an additive liner regression model[46].

Size estimation of fat cells. Fat beds were collected from mice shortly after culling them. The beds were transferred to a 4% paraformaldehyde (PFA)-based fixing solution and sent to histology for paraffin-embedding. The paraffin blocks were cut to a central core (estimated as closest to midway through the fat pad), then cut to 4-µm sections and mounted onto microscope slides for staining with haemotoxylin and eosin. Images were captured by using an Eclipse E800 camera (Nikon): QICAM Fast1394 (QImaging) supported by an automated Stage (ProScan II, PRIOR Scientific) for random selection. Images were generated using Image Pro Plus 7.0 software. Twenty high-magnification images (10× to 40×, depending on cell size) of the tissue were randomly selected using the ProScanII random-selection facility. From six individual imaged sections cut across a fat pad from a given mouse, six of the largest visible whole cells in each field of known area were selected and used to estimate the average cross-sectional area of the cells from that fat bed for each mouse, measured as μm^2/cell (average of 36 random cell bodies).

Glucose and insulin tolerance tests, and *in vivo* NEFA release. Glucose tolerance was determined by oral or intraperitoneal administration of D-glucose (2 mg per g body weight (mg/g)) after a 6-h fast. Insulin tolerance was determined by intraperitoneal injection of humulin S (0.5–2.0 mU per g body weight (mU/g)) (for insulin-resistant *Lepr* mutants) after a 4-h fast. Lipolytic responsiveness was determined by injection of 1 µg/g CL316,243 after a 5-h fast. In all of the cases, blood was sampled before administration of the test substance ($t = 0$ min) and then generally at 15, 30, 60 and up to 120 min later (for GTT). Glucose was measured from a tail venesection using a hand-held glucometer (OneTouch, Lifescan, Milpitas, USA) and insulin (Crystalchem ELISA, Chicago, USA) or NEFA (Wako, Richmond VA, USA) was measured in plasma that was prepared from blood collected in EDTA-coated microtubes (Sarsted, Leicester, UK).

Euglycemic hyperinsulinemic clamps. Male C57BL/6N or Adipoq-Tst littermates were fed a high-fat diet for 2 weeks. Mice were anesthetized with isofluorane (5% induction, 2% maintenance in 2% oxygen) and a mirocrenathane cannula was implanted in the right exterior jugular vein and exteriorized at the back of the neck. Mice were injected with 0.05 mg/kg buprecare subcutaneously (buprenorphine) at the start of surgery and were given rimadyl (0.001% vol/vol) in their drinking water overnight on the first day after surgery. Clamps

were performed 3 d after jugular cannulation. Mice were fasted overnight, and body weight, lean and fat mass were determined by time domain–nuclear magnetic resonance (TD-NMR) (Bruker LF50; http://www.bruker.com). All mice were infused for 2 h with 0.05 μCi/min D3-[^{3}H]glucose (NET331C005MC, PerkinElmer; http://www.perkinelmer.com) to assess endogenous glucose production by sampling shortly before the clamp procedure (−5 min). The clamp was started with infusion of higher-specific activity tracer (0.1 μCi/min) and a prime of insulin (humulin S; Eli Lily) at 9.0 mU per kg lean mass per min for 3 min, followed by a constant infusion of insulin at 2.5 mU per kg lean mass per min and a variable infusion of 20% glucose. Blood glucose was sampled from 20 min until 60 min to achieve a steady-state blood glucose level at ~7.6 mmol/liter. A bolus of 10 μCi [2-^{14}C]deoxyglucose (NEC495001MC, PerkinElmer) was administered at 75 min, and samples were taken from the cut tail for tracer and glucose analysis at 80, 85, 90, 100, 110 and 120 min. Insulin levels were measured from basal (−5 min) and clamp (100 min) time points. Mice were euthanized with euthatal, which was administered down the cannula, and tissue (quadriceps muscle and epididymal fat) was rapidly excised. Tissues were weighed and extracted in 10 volumes of water; the phosphorylated [2-^{14}C]deoxyglucose was recovered using Poly-Prep columns, AG 1-X8 anion exchange columns (Bio-Rad). Tracers were used to calculate various aspects of glucose metabolism[47]. Tissue glucose clearance was (K_g) calculated by dividing the column-recovered tissue-phosphorylated [2-^{14}C]deoxyglucose by the area under the curve of plasma [2-^{14}C]deoxyglucose (trapezoidal method). K_g was used to calculate a metabolic index (R_g), a measure of tissue-specific glucose uptake, and is the product of K_g and the mean glucose concentration over the clamp period[47]. Plasma tracers were measured after deproteinization with $Ba(OH)_2$ and $ZnSO_4$. Plasma glucose/tracers were measured after drying the sample and were used to calculate specific activity and rates of disposal (R_d)/endogenous production (EndoR_a)[47]. The wet sample containing $3H_2O$ was used to estimate glycolytic rates. Tracers were counted using Prosafe FC + High-Efficiency LSC cocktail (Meridian Biotechnologies Ltd) in a TriCarb 2100TR β-scintillation counter (PerkinElmer) with a dual ^{3}H/^{14}C program.

Antibodies (dilutions) used for this study. Donkey anti-goat IRDye 680RD (1: 10,000; 926-68074), donkey anti-mouse IRDye 680RD (1: 10,000; 925-68072) and goat anti-rabbit IRDye 800CW (1: 10,000; 926-32211) were from Licor Biosciences Ltd. Goat anti–aconitase 2 (1: 10,000; Ab99467), rabbit anti–aconitase 2 (1: 50,000; Ab129069), goat anti-aconitase 1 (1: 500; Ab10694), complex II antibody Cocktail (1: 250; Ab110410), rabbit anti-Glut4 (1: 2,000; Ab654), rabbit anti-SDHB (1: 1,000; Ab84622) and rabbit anti-TST (1: 2,000; Ab60128) were from Abcam. Rabbit anti-SDHB (1: 7,000; NBP1-54154), rabbit anti-SOD2 (1; 2,000; NBP1-40422) and goat anti-SOD1 (1: 10,000; NB100-60944) were from Novus Biologicals. Rabbit polyclonal anti-TST antibody (1: 1,000; GTX 114858) was from Source Biochemicals. The activation state of HSL and other lipolytic protein levels were investigated using the lipolysis activation antibody sampler kit (Cell Signaling, cat number 8834), with dilutions according to the manufacturer's instructions.

Clonal adipocyte cell experiments. The 3T3-L1 preadipocyte cell line was obtained from the American Type Culture Collection. The Expression Arrest GIPZ lentiviral shRNAmir-mediated plasmid-based system (Open Biosystems, Epsom, UK) was used to transduce mature 3T3-L1 adipocytes (days 6–8 of differentiation) to knock down *Tst* (**Supplementary Fig. 7f**). Mitochondrial ROS studies were performed by exposing the transduced 3T3-L1 cells to medium containing 1% H_2O_2 for 6 h, followed by, after careful rinsing, exposure to Mitotracker Red-CM-H_2XROS (final concentration 250 nM; M7513; Molecular Probes, Invitrogen, Paisley, UK). Probe oxidation was quantified using an M1000 fluorescence reader and Magellan software (Tecan, Reading, UK). Human Simpson–Golabi–Behemel syndrome (SGBS)[32] human clonal preadipocytes were maintained at 37 °C, 5% CO_2 in Dulbecco's modified Eagle's medium (DMEM)/F12 supplemented with 10% (vol/vol) FBS, 50 U/ml penicillin, 50 μg/ml streptomycin, 33 μM biotin and 17 μM pantothenic acid, and differentiated with the addition of 0.5 mM isomethylbutylxanthine (IBMX), 0.25 μM dexamethasone, 20 nM insulin, 2 μM rosiglitazone, 0.01 mg/ml transferrin, 0.1 μM cortisol and 200 pM triiodothyronine (T3). From day 7 to day 21, cells were differentiated without IBMX and dexamethasone. Neither cell line was tested for mycoplasma during these studies.

***TST* gene expression during human preadipocyte differentiation.** Isolated omental (Om) and subcutaneous (SC) preadipocytes (Zen-Bio Inc., Research Triangle Park, NC, USA) were cultured as previously described[31]. The differentiation was routinely monitored by measuring fatty acid synthase and adiponectin expression (FASN, Hs00188012_m1 and Adipoq, Hs00605917_m1).

Preparation of primary adipocytes and lipolysis. Adipocytes were prepared from mice as follows. Mice were culled, and epididymal fat was removed into warmed Krebs buffer (118 mM NaCl, 5 mM KCl, 1.2 mM $MgSO_4$, 10 mM $NaPO_4$, pH 7.4, 1% BSA, 1 mg/ml glucose, 1.25 mM $CaCl_2$). The tissue was then cut with sharp scissors into approximately 2- to 4-mm-diameter pieces in Krebs buffer with 2 mg/ml collagenase I (Worthington Lot: 43C14114B). Fat fragments were incubated at 37 °C in a cell culture incubator for 40–50 min. The suspension was mixed by swirling every 10 min. Digestion was stopped when the majority of material was visible as dissociated adipocytes. The cell suspension was passed through a 250-μm mesh into a 50-ml Falcon tube to remove undigested material. An equal volume of experimental medium (1× DMEM, 4.5 g/liter glucose, 4 mM glutamine, 100 U/ml penicillin–streptomycin, 10% charcoal-dextran-stripped FBS) was added to the suspension, before centrifugation at room temperature for 3 min (1,500*g*). Adipocytes, which accumulate at the top of the suspension, were removed into 5 volumes of fresh experimental medium, using a cut 1-ml pipet tip. Adipocytes were swirled and given 5 min to settle to the top. Medium was removed from below the adipocyte layer, and another 5 volumes of medium was added. Cells were incubated for 60 min at 37 °C and 5% CO_2. Cells were then given a third wash, and after removal of the medium, the adipocytes were added to their experimental tubes. For basal lipolysis, 35 μl of adipocytes were transferred to 300 μl experimental medium in a 500-μl microcentrifuge tube with open lids to maintain oxygenation of adipocytes. Tubes were gently shaken to mix the adipocytes before incubating them in a 37 °C incubator (5% CO_2). After 90 min, the tubes were gently shaken once more. The tubes were left still for 1 min to allow the adipocytes to resettle before samples were taken carefully from below the adipocyte layer with a catheter-linked microsyringe. For CL stimulation, CL316,243 was added in a volume of 15 μl of experimental medium to the adipocyte suspension, to a final concentration as indicated for each experiment. Tubes were gently shaken to mix the suspension, and tubes were returned to the incubator for 30 min. At this time, the tubes were gently shaken before taking samples of the medium. The tubes were returned to the incubator for a further 90 min. Tubes were shaken once more before final sampling, as described above.

NEFA assay. Standards and samples of 40 μl were incubated with WAKO NEFA kit with 100 μl of Reagent 1 (5 min, 37 °C) in a clear, flat-bottom plastic 96-well assay plate. 50 μl of Reagent 2 was then added, and the sample was incubated for another 5 min. Absorbance of each sample was read at 565 nm, with a background correction at 660 nm. A standard curve (which is linear between 5 μM and 250 μM) was prepared from a 1-mM reference sample (Wako).

Lipogenesis assay. Adipocytes were prepared as for the lipolysis assay described above. Experimental medium (±insulin, ±10 μM cytochalasin B (glucose uptake inhibitor as a negative control)) was prepared by adding [^{3}H]glucose to a final concentration of 0.5 μCi/ml. The typical ratio of medium/cells was 5/1 by volume. Medium (+ [^{3}H]glucose) was added to a plastic scintillation vial, and then adipocytes were added. Cells and medium were mixed and incubated for 2 h in an incubator at 37 °C with 5% CO_2 and gentle shaking every 15 min. 6 M H_2SO_4 (1 μl/10 μl of experimental medium) was added, and the sample was vortexed for 30 s to stop the reaction. Organic scintillant (two volumes per volume of medium) was added without mixing and left standing for >4 h to allow the lipids to diffuse into the organic scintillant layer. Incorporation into lipid was calculated using a ^{3}H-sensitive scintillation counter (with corrections using a no-cell blank, a cell blank and cytochalsin B ([^{3}H]glucose background)) and normalized to lipid mass, which was calculated by extraction of parallel samples in extraction solvent (4:1:1, isopropanol:heptane:1 N sulfuric acid). For each 100 -μl adipocyte suspension, 1.5 ml of water, 2.5 ml of extraction solvent and 1.5 ml of heptane were added, followed by solvent evaporation and accurate mass determination on a fine balance.

doi:10.1038/nm.4115

Glycated hemoglobin A1c (HbA1c) levels. HbA1c levels were measured by reverse-phase cation-exchange chromatography by using the Evolution HA-8160 automated analyzer (A. Menarini Diagnostics Ltd., Wokingham, UK) according to the manufacturer's instructions. Briefly, 3.4 µl of diluted lysed whole blood was injected onto the stainless steel Arkray column, which consisted of a prefilter and an analytical column packed with an ion-exchange resin (a hydrophilic polymer of methacrylate ester copolymer). Elution was achieved with a five-step phosphate-buffered gradient with increasing ionic strength, using three buffers (80A, 80B and 80CV). Hemoglobin fractions were detected with a dual-wavelength (420–500 nm) LED photodiode. The instrument was calibrated with two calibrators. The reported result is derived from the ratio HbA1c/total HbA, adjusted for calibration. Within-run and between-run coefficient of variation were both <3.0%.

Mitochondrial functional tests. Mitochondria were extracted from the livers of fed male adult C57Bl6 or *Tst*$^{-/-}$ mice. Livers that were rapidly excised after the mice were humanely killed were placed in ice-cold isolation buffer (IB: 10 mM Tris–MOPS (3-(*N*-morpholino)propanesulphonic acid), 1 mM EGTA in Tris, 200 mM sucrose, pH 7.4; all from Sigma-Aldrich). All further steps were performed on ice or at 4 °C (centrifugation). Whole livers were minced by using scissors, washed in ice-cold IB buffer and then homogenized in 5 ml IB buffer by using a glass Potter Elvehjem homogenizer. Homogenates were transferred to 50-ml Falcon tubes (polypropylene Falcon tube, Corning) and centrifuged at 1,800 r.p.m. for 10 min (Heraeus Megafuge 1.0R). Supernatants were transferred to Beckmann ultracentrifuge glass tubes (Beckman, USA) and were further centrifuged at 7,800 r.p.m. for 10 min in a Beckman J2-MC ultracentrifuge (Beckman, USA). Supernatants were discarded, and the remaining pellet was washed with 5 ml ice-cold IB buffer before being centrifuged again at 7,800 r.p.m. for 10 min. Finally, the supernatants were again discarded and the pellets were resuspended by using a glass rod and by gentle pipetting. This represented a purified mitochondrial preparation. Protein concentration was determined by a Bradford protein assay, and all experiments were performed at a final concentration of 0.2 mg/ml protein. Mitochondrial preparations were injected directly into an Oroboros Oxygraph 2K (Oroboros Instruments, Austria) high-resolution respirometer, using Hamilton microsyringes (Hamilton, UK). Prior to this, the two chambers of the Oxygraph 2K were filled with MiR-05 buffer that was designed to support optimal respiration (0.5 mM EGTA, 3 mM $MgCl_2.6H_2O$, 60 mM K-lactobionate, 10 mM KH_2PO_4, 20 mM HEPES, 110 mM sucrose, 1 g/liter BSA, pH 7.1; all reagents were from Sigma-Aldrich) and were allowed to normalize with room oxygen concentrations for a minimum of 1 h, minutes before closing the chambers. Oxygen concentration of the chambers and rate of oxygen use (respiration) were recorded by using DataLab software (Oroboros). All further substrates or reagents, including 2.5 mM malate, 5 mM pyruvate, 2 µM rotenone (complex I inhibition for complex II-specific assessment), 10 mM succinate, 100 µM ADP and 1 µg/ml oligomycin (all Sigma-Aldrich) were added into the chamber directly by using microsyringes (Hamilton). Na_2S (from Sigma) pre-incubation was for 2 h on ice in the undiluted mitochondrial fraction before assessment of mitochondrial function.

Blood sulfide measurement. Determination of hydrogen sulfide concentration in whole-blood samples was performed by derivatization with monobromobimane (mBBr) followed by HPLC separation and detection with a fluorescence detector. Briefly, for each blood sample to be derivatized, one 1.5-ml brown glass vial was labeled and filled with 100 µl of 160 mM EPPS in 16 mM diethylenetriaminepentaacetic acid (DTPA) pH 8.0, followed by 100 µl of acetonitrile and 10 µl of 46 mM mBBr solution in acetonitrile. To this solution, 50 µl of blood (immediately withdrawn from a mouse) was dispensed, and the reaction vials were capped tightly and vortexed for 10 min. Subsequently, 1 ml ethyl acetate was added, and the tube was capped and vortexed for another 10 min. After this, the reaction vials were centrifuged gently at 350*g* for 7 min to separate aqueous and organic layers. The organic layer was collected from each extraction and transferred to a 1.5-ml brown glass vial, and the solvent was evaporated completely under a nitrogen stream. Acetonitrile (200 µl) was added to each vial, and the solvent was again evaporated to remove any traces of ethyl acetate. To quantify sulfide dibimane in a sample, the dried residue was resuspended in 50 µl of buffer A (10 mM tetrabutylammonium phosphate aqueous, 10% methanol, 45 mM acetic acid adjusted to pH 3.4). The entire sample was transferred to an HPLC autosampler vial with a 200-µl glass sample insert, and the vial was closed with a penetrable cap. 20 µl of the sample was injected onto a C8 reverse-phase column (LiChrospher 60 RP-select B 5 µm, 4.0 × 125 mm LiChroCART 125-4, Merck KGaA) and a guard column (LiChroCART 10-2, Superspher 60 RP-select B cartridge) on an Ultimate 3000 UHPLC+ focused system (Thermo Scientific). Sulfite dibimane was eluted with a linear gradient from 10% buffer B (10 mM tetrabutylammonium phosphate in methanol, 10% water, 45 mM acetic acid) to 100% buffer B over 30 min. The eluent was analyzed by fluorescence (λ_{ex} = 380 nm, λ_{em} = 480 nm).

Human adipose tissue analysis. For cohort 1, samples of visceral (omental) and subcutaneous adipose tissue were obtained from white female subjects who were morbidly obese (BMI > 40 kg/m^2) and who had undergone laparoscopic bariatric surgery and from lean to overweight control subjects (BMI < 30 kg/m^2) who had undergone other elective laparoscopic surgeries at the General Hospital of Vienna (n = 8 per subgroup). This group size was initially chosen as it had revealed consistent changes in gene expression between samples of visceral and subcutaneous fat in previous analyses. Criteria for exclusion were the presence of any infectious, inflammatory, neoplastic or systemic disease, diabetes (excluded by fasting plasma glucose levels or the use of antidiabetic drugs), or other uncontrolled endocrine diseases. None of the individuals used antibiotics, anti-inflammatory, anti-obesity or lipid-lowering drugs when participating in the study. The study was approved by the ethics committee of the Medical University and the General Hospital of Vienna. For cohort 2, subcutaneous adipose tissue was obtained from a large cohort[30] of Icelandic subjects (n = 670). Cohort size was predefined[30]. For cohort 3, a group of 180 adipose tissue samples (96 visceral and 84 subcutaneous depots) from participants with a body mass index (BMI) within 20 and 68 kg/m^2, who were recruited at the Endocrinology Service of the Hospital Universitari by Dr. Josep Trueta (Girona, Spain), were analyzed[31]. Cohort size was predfined[31]. Ethics related to the sampling in Spain and Iceland are detailed in the respective references[30,31], and all studies were done with informed consent according to the relevant designations and/or country guidelines. Significance of correlational data for *TST* and other adipose genes was assessed with Scheffé *post hoc* tests (**Supplementary Table 4**).

Additional gene expression. RNA extraction, cDNA synthesis and real-time PCR were performed as described[8,31]. Probes were mouse *Tst*, Mm00726109_m1; *Gapdh* (internal control), Mm99999915_g1; and *Tbp* (internal control), Mm0000446973_m1. *Prx3*, Mm00545848_m1; *Slc2a4* (*Glut4*), Mm00436615_m1; *Cpt1a*, Mm01231183_m1; *Adrb3*, Mm02601819_g1; *Pparg*, Mm00440940_m1; *Cebpd*, Mm00786711_s1; *Cebpb*, Mm00843434_s1; *Cebpa*, Mm00514283_s1; *Dlk1*, Mm00494477_m1; *Klf5*, Mm00456521_m1; and *Srebp1*, Mm00550338_m1. Human *TST* was measured by using Hs00361812_m1, and *TBP* was measured with Hs99999910_m1.

TST activity assays. The adapted TST assay[48] was performed in a 96-well plate with tissue homogenates. The reaction was started by the addition of 10 µl 500 mM KCN (final concentration 50 mM). The reaction proceeded for 20 min and was stopped by the addition of formaldehyde (63 µl of reaction mix into 7 µl formaldehyde). The colormetric change was achieved by the addition of 30 µl 300 mM $Fe(NO_3)_3$ (final concentration 30 mM), which quickly underwent ligand exchange with thiocyanate to give the consequent color change from yellow to red. The absorbance was measured at 460 nm and TST activity was corrected for non-enzymatic activity. A standard curve was produced by addition of thiocyanate (SCN) (1.8 mM to 0.025 mM) to $Fe(NO_3)_3$. From the standard curve the relative concentrations of $^-$SCN produced could be calculated, and therefore the turnover of TST activity with the compounds could be determined. A recombinant human TST preparation was tested in parallel to infer non-TST-mediated substrate turnover.

Statistical analyses and approaches. For gene expression, hormone levels and protein levels, group sizes of 6 were generally used for calculations, to allow detection of differences in these variable parameters to a threshold of 15% (there is sufficient power to detect smaller differences in certain parameters with this cohort size) with a power of at least 0.8. In some studies, limitations in animal numbers, or fewer remaining samples from larger group sizes resulting from

their use for multiple end-points, precluded the desired minimum of $n = 6$ per group. Protein or mRNA differences in validation studies with two parameters (for example, diet with mouse line or genotype) were analyzed using two-way ANOVA for line and diet effects, followed, where appropriate, by *post hoc* Tukey tests or Holm–Sidak multiple comparison tests using Sigmastat version 3.5 (Systat Software) or Prism (GraphPad Software). For simple two-condition comparisons, a Student's *t*-test was used. For simple comparisons of control versus treated mice (including different treatments or concentration-response curves), data were analyzed by one-way ANOVA. For longitudinal measures (for example, GTT, ITT and body-weight gain), repeated measures (RM) ANOVA was used and multiple comparisons were determined. The statistical model for the analysis of F_2 mouse cross data were as described above and in previous studies[6]. Parameters and other statistical quantities were inferred using Markov chain Monte Carlo (MCMC) methods as used in the MCMCpack R package. Data were normally distributed. For all main *in vivo* studies, a blinding strategy was used in which the operator (for example, for injections of glucose or administration of drug) was blinded to the genotype of the subject during the experiment. Similarly, for analysis of images (for example, fat-cell size), the scorer was blinded to genotype and the data coded; the code was subsequently broken by a second individual. Downstream analysis of, for example, tissue mRNA and protein content, was generally not done in a blinded manner, so that appropriate data arrangement on, for example, representative western blots, could be done.

46. Munger, S.C. *et al.* RNA-seq alignment to individualized genomes improves transcript abundance estimates in multiparent populations. *Genetics* **198**, 59–73 (2014).
47. Steele, R., Wall, J.S., De Bodo, R.C. & Altszuler, N. Measurement of size and turnover rate of body glucose pool by the isotope-dilution method. *Am. J. Physiol.* **187**, 15–24 (1956).
48. Hildebrandt, T.M. & Grieshaber, M.K. Three enzymatic activities catalyze the oxidation of sulfide to thiosulfate in mammalian and invertebrate mitochondria. *FEBS J.* **275**, 3352–3361 (2008).

doi:10.1038/nm.4115